MIXED CONVECTION FLOW AND HEAT TRANSFER PHENOMENA ACROSS TRAPEZOIDAL BLUFF BODIES: A COMPARATIVE STUDY

A DISSERTATION

Submitted in partial fulfillment of the

requirements for the award of the degree

of

INTEGRATED DUAL DEGREE

(Bachelor of Technology & Master of Technology)

in

CHEMICAL ENGINEERING

(With Specialization in Hydrocarbon Engineering)

By

VIVEK KUMAR VERMA

DEPARTMENT OF CHEMICAL ENGINEERING

INDIAN INSTITUTE OF TECHNOLOGY ROORKEE

ROORKEE-247 667 (INDIA)

MAY, 2014

CANDIDATE'S DECLARATION

I hereby declare that the work, which is being presented in this dissertation entitled **"Mixed Convection Flow and Heat Transfer Phenomena Across Trapezoidal Bluff Bodies: A Comparative Study "** in partial fulfillment for the requirements of the award of the degree of Integrated Dual Degree (Bachelor of Technology & Master of Technology) in Chemical Engineering with specialization in "Hydrocarbon Engineering", submitted in the Department of Chemical Engineering, Indian Institute of Technology Roorkee, is authentic record of my own work carried out during the period May 2013 to May 2014, under the supervision of **Dr. Amit Kumar Dhiman**, Associate Professor, Department of Chemical Engineering, Indian Institute of Technology Roorkee, Roorkee. The matter embodied in this work has not been submitted for the award of any other degree.

Date:

Place: IIT Roorkee **(VIVEK KUMAR VERMA)**

CERTIFICATE

This is to certify that the above statement made by the candidate is correct to the best of my knowledge.

Dr.Amit Kumar Dhiman
Associate Professor
Department of Chemical Engineering
IIT Roorkee

ACKNOWLEDGEMENT

I would like to express my thanks to Dr. Amit Kumar Dhiman, Associate Professor, Department of Chemical Engineering, Indian Institute of Technology Roorkee, for his inspiration and constant encouragement to work on this project. It would not have been possible for me to complete the project without the support of Dr. Dhiman.

I would also like to thank my colleagues/scholars, who also work in the same laboratory for their valuable suggestions and help as and when required.

Above all, I want to express my heartiest gratitude to The Almighty, my parents (Mrs. Rita Verma and Mr. Binod Verma), for their love and support for me, which has always been a constant source of inspiration.

VIVEK KUMAR VERMA

CONTENTS

LIST OF FIGURES

LIST OF TABLES

Abstract

Two-dimensional numerical simulations have been realized to explore and evaluate the laminar mixed convection flow and heat transfer across a heated trapezoidal bluff body in an unconfined domain. Two different configurations of the trapezoidal bluff body viz. expanded and tapered have been considered and a comparison has been evaluated at different operational parameters. The spectrum of physical control parameters considered as Reynolds number (Re)=10-50, Richardson number (Ri)=0-1 and Prandtl number (Pr)=0.7 (air). A finite volume method implemented on the collocated grid arrangement has been employed for numerical computations. The flow and heat transfer characteristics have been represented by streamline and isotherm contours respectively at varying values of Re and Ri**.** Drag and lift coefficients for the tapered body is found higher as compared to the expanded body for same operating conditions. However, average Nusselt number is greater for an expanded body as compared to a tapered body. With increase in Re at a given Ri, drag coefficient is found to decrease in steady regime, but it increases in time-periodic regime. On advancing Ri, drag and lift coefficients decrease for the steady state regime for both the geometries. A correlation expressing the functional relationship of average Nusselt number with Re and Ri for both geometries have been proposed. Critical Reynolds number at Ri=0.5 for the expanded geometry is found to be between Re=46 and 47, while for the tapered body it is found to be between Re=35 and 36. Maximum heat transfer enhancement for the expanded body at Ri=0.5 and Ri=1 with respect to Ri=0 is found to be approximately 8.5% and 2% respectively. Similarly, for the tapered body maximum augmentation in heat transfer for the above mentioned conditions is found to be approximately 6% and 2%. Maximum heat transfer enhancement for the tapered body with respect to the expanded body at Ri=0, 0.5 and 1 is found to be approximately 26%, 24% and 21% respectively.

Keywords: Cross-buoyancy; Expanded trapezoidal cylinder; Tapered trapezoidal cylinder; Drag coefficient; Lift coefficient; Richardson number; Nusselt number; Critical Reynolds number.

Nomenclature

a	anterior and posterior edge of expanded and tapered trapezoidal bodies respectively, m
b	posterior and anterior edge of expanded and tapered trapezoidal bodies respectively, m
c_p	specific heat capacity of fluid, J kg^{-1} K^{-1}
C_D	overall drag coefficient ($= 2F_D / \rho U_\infty^2 b$)
C_{DF}	frictional drag coefficient ($= 2F_{DF} / \rho U_\infty^2 b$)
C_{DP}	pressure drag coefficient ($= 2F_{DP} / \rho U_\infty^2 b$)
C_L	overall lift coefficient ($= 2F_L / \rho U_\infty^2 b$)
f	frequency of vortex shedding, s^{-1}
F_D	overall drag force per unit length of the cylinder, N m^{-1}
F_{DF}	frictional drag force per unit length of the cylinder, N m^{-1}
F_{DP}	pressure drag force per unit length of the cylinder, N m^{-1}
F_L	lift force per unit length of the cylinder, N m^{-1}
g	acceleration due to gravity, m s^{-2}
h	local heat transfer coefficient, W m^{-2} K^{-1}
$\bar{h}$	average heat transfer coefficient, W m^{-2} K^{-1}
H	height of the computational domain, m
k	thermal conductivity of the fluid, W m^{-1} K^{-1}

L	length of the computational domain, m
Nu	local Nusselt number (= hb/k)
$\bar{Nu}$	average Nusselt number (= $\bar{h}b/k$)
p	pressure, Pa
Pr	Prandtl number (= $\mu c_p / k$)
Re	Reynolds number (= $\rho U_\infty b / \mu$)
Ri	Richardson number (=gβ(T_w-T_∞)b/U_∞^2)
St	Strouhal number (= fb/U_∞)
T	temperature, K
T_∞	temperature of the fluid at the inlet, K
T_w	constant wall temperature at the surface of the cylinder, K
t	time, s
U_∞	free stream velocity at the inlet, m s^{-1}
V_x	velocity component in the x-direction
V_y	velocity component in the y-direction
X_d	downstream distance, m
X_u	upstream distance, m
x	streamwise coordinate
y	transverse coordinate

Greek symbols

θ	dimensionless temperature (= (T-T_∞)/(T_w-T_∞))
μ	viscosity of the fluid, kg m^{-1} s^{-1}
ρ	density of the fluid, kg m^{-3}
β	coefficient of volumetric expansion, K^{-1}

Paper Communicated In Journal

- Vivek Kumar Verma, Amit Dhiman, Cross-Buoyancy Mixed Convection Across Expanded and Tapered Trapezoidal Bluff Bodies-A Comparative Study.

International Journal of Heat and Mass Transfer

CHAPTER-1

INTRODUCTION

An ample of research has been conducted to examine the formation of vortex and the phenomenon of vortex shedding around a bluff body because of various prodigious applications. Vortex formation has been used to generate voltage by installing a piezoelectric device in the vortex formation zone. Oscillation of vortex creates fluctuation in pressure and hence stress on piezoelectric device which generates voltage due to varying stress on it. Most vital application of vortex shedding is involved in designing of vortex flow meters in which frequency of vortices generated is used to calculate flow rate of fluid. Vortex shedding phenomena has utilization in designing of weather buoys, in which the buoys placed on surface of water create vortex and by observing the vortex properties wind speed is evaluated. Vortex shedding by a bluff body has application in designing of heat exchange systems, where it is desired to enhance formation of eddies and vortices so as to augment heat transfer rate. The flow and thermal patterns depend on object size, geometry of object, velocity of fluid, external parameters, orientation of object with respect to flow, type of flow whether confined or unconfined, properties of fluid, properties of object and others. Flow and heat transfer phenomena become even more intricate when buoyancy forces and gravity are also taken account for. It is obvious that the values of output parameters such as drag coefficient, Nusselt number, wake size, etc. vary from one regime to another and these parameters show dependence on the Reynolds number(Ri), Prandtl number(Pr) and Richardson number (Ri). Particularly, the shape of the obstacle has a formidable effect on the transport processes and the resultant momentum and thermal dynamics. In the present case, effects of cross-buoyancy (Ri) and Re on fluid flow and heat transfer have been analyzed for two different configurations of trapezoidal cylinder viz. expanded and tapered. It is worthwhile to mention that the mixed convection heat transfer from a heated trapezoidal cross-section has received virtually no attention in the literature.

1.1 Terminology

- **Bluff Body**- Drag on a body due to an external flow of fluid has two components namely drag due to wall shear stress and drag due to pressure gradient. If drag due to pressure is more significant than drag due to shear, then the obstacle is referred as bluff body.

Whereas if drag due to shear dominates then it is called a streamline body. In a bluff body flow separation takes place quite early this creates low pressure region downside of object and hence drag due to pressure increases.

- **Newtonian Fluid**- In a fluid if stress acting on the surface is directly proportional to strain rate, then that fluid is called Newtonian fluid. Constant of proportionality for Newtonian fluids is viscosity which is independent of stress. No real fluid is Newtonian in exact terms but air and water can be approximated to be Newtonian for normal range of operation.

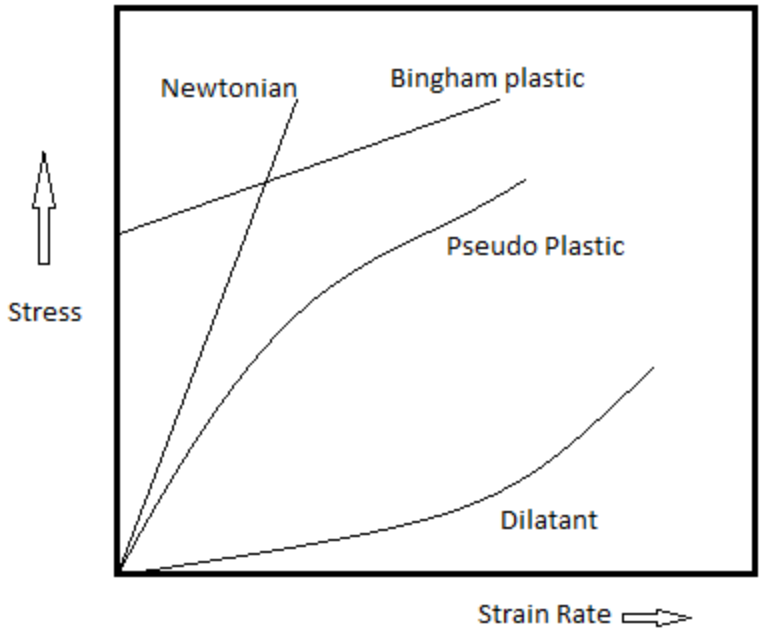

Figure 1: Dependence of stress on strain rate for various types of fluid.

- **Flow separation**-It is a process by which at higher Reynolds number fluid particles does not remain attach to the solid surface and gets detached from the surface. When fluid collides with frontal edge of body, particles near the surface comes to rest and hence relatively high pressure develops in this region. As we move along the surface pressure decreases and hence because of negative pressure gradient fluid flows along the surface even though viscous force tends to oppose it. At rear end there is positive pressure

gradient also called adverse pressure gradient which opposes the flow and hence, at a point where convective force outweighs viscous force then fluid particles leave the surface. As a result of flow separation, region of low pressure forms behind the body and causes formation of vortices.

- **Steady Flow**- If the flow properties of fluid are constant with time then this type of flow is called steady flow. Steady flow generally happens in low Reynolds number and the flow becomes unsteady in high Reynolds number region. In unsteady state there is variation in physical and thermal patterns with time.

1.2 Dimensionless Numbers

- **Nusselt number (Nu)** - It physically represents ratio convective heat transfer to conductive heat transfer. Mathematically it is calculated as-

  $$Nu=(h*l)/k$$

  where h=heat transfer coefficient

  l=equivalent length

  k=thermal conductivity

  Higher Nu represents high heat transfer rate by convection as compared to conduction.

- **Strouhal number (St)** - It describes the oscillating behavior of fluid flow and this property is pertinent only to unsteady flow. It is given as-

  $$St=fD/U_{\infty}$$

  where f is frequency, D is diameter of obstacle and U_{∞} is free stream velocity.

  Higher St represents more fluctuations in system i.e higher frequency.

- **Prandtl number (Pr)** -It is the ratio of momentum diffusivity to thermal diffusivity.

  $$Pr=\mu C_p/k$$

  where μ is viscosity, C_p is specific heat and k is thermal conductivity.

For Pr higher than one, momentum boundary layer is above thermal boundary layer and vice versa. Pr represents only property of fluid and does not indicate anything about flow property. For air, value of Pr is 0.7.

- **Reynolds number (Re)** - It is the ratio of inertial force to viscous force. Higher Re signifies large inertial force as compared to viscous force.

  $$Re = \rho U_\infty b / \mu$$

  where ρ is density, U_∞ is free stream velocity, b is equivalent length, μ is viscosity.

  At large Reynolds number, when viscous force is unable to restrict inertial force, turbulence flow takes place.

- **Grashof number (Gr)** - It represents the ratio of buoyancy force to viscous force. At higher Grashof number heat transfer primarily occurs due to pure convection happening due to effect of buoyancy.

  $$Gr = g\beta(T_s - T_0)L^3 / \nu^2$$

  where β=coefficient of volumetric expansion

  g=acceleration due to gravity

  L=characteristic length

  T_0=ambience temperature

  T_s=surface temperature

  ν =kinematic viscosity

- **Richardson number (Ri)** - It represents the ratio of natural convection to forced convection. If Ri is close to zero then forced convection dominates and if it is larger than one then free convection predominates and buoyancy effect comes in play. Mathematically Richardson number is given as-

  $$Ri = Gr/Re^2$$

  For Ri=0, implies forced convection.

  For Ri=∞, implies pure natural convection.

CHAPTER-2

LITERATURE REVIEW

In context of shape of bluff body suitable for use in vortex flow meter a detailed analysis of the various methods of investigating phenomena of the vortex flow meters have been performed by Pankanin [1] and concluded that the bluff body most suitable for the design of this type of flow meters is a tapered trapezoidal cylinder. Steggel and Rockliff [2] adumbrated the fallout of body geometry on vortex shedding behavior of bluff body by analyzing viscous flow around rectangular bodies by considering various side ratio, angle of incidence and Reynolds number. They pointed out that shape of body has humungous effect on shedding behavior. Miau et al. [3] made a comprehensive study on fluctuation at low frequency in the wake region of trapezoidal cylinder with low aspect ratio and high Reynolds number. Xing et al. [4] performed numerical simulations to optimize the bluff body shape for increasing the efficiency of a vortex flow meter and observed trapezoidal cylinder serves the purpose best. El-Wahed et al. [5] performed a study of vortex ejection from different types of bluff bodies. They mentioned that regular vortex shedding is rapidly achieved in case of tapered trapezoidal bluff body as compared to cylindrical, rectangular, triangular and T-shape shedders. Venugopal et al. [6] carried out the investigations on vortex flow meter with a unique technique of differential wall pressure measurement method and emphasized that a tapered trapezoidal geometry gives best results. A trapezoidal body has been used in piezoelectric sensors by Wang et al. [7]. A trapezoid has been used to construct ultrasound probe used for diagnosis. Gee et al. [8] presented a novel technique for three-dimensional ultrasound probe calibration. The probe, scan plane and imaging array used were a trapezoid.

The vortex shedding from trapezoidal cross-section type body has experimentally been investigated by Goujon-Durand et al. [9]. They elucidated the scaling laws for the prognosticating velocity oscillation in the wake behind of the obstacle. Hulin et al. [10] studied the vortex emission behind cylindrical shaped obstacle with trapezoidal cross-section in two phases (air and water) for vertical flow and verified the observations with optical fiber probe measurements. Lee [11] studied the primal stages of the wake flow developments around a tapered trapezoidal obstacle for Re=25-1000. Initially there is no separation observed but with time a perfectly symmetric wake develops behind obstacle. Chung and Kang [12] studied the

variation of Strouhal number with Re (100, 150, and 200) and height ratio (0.7 and 0.85). They observed that St has its minima at height ratios of 0.7 and 0.85 for Re 100 and 150, respectively. The movement of the flow separation point from the rear to front corners and the change of secondary vortex strength are important factors in determining the shedding structures for Re 100 and 150. However, no information is available on drag and lift coefficients. Kahawita and Wang [13] numerically computed the Benard von Karman hydrodynamic instability behind tapered trapezoidal bluff bodies using the spline method of fractional steps. They also stated that a trapezoidal shape is more desirable than a cylinder, since well-defined vortex emission due to clean separation at its sharp edges is assured. Venugopal et al. [14] in another study carried out experimental investigations on the vortex flow meter with the differential wall pressure measurement method. They demonstrated that the vortex flow meter comprising of a trapezoidal cross-section is one of the major contributors in the field of flow metering. In recent times, Dhiman and Hasan [15] demonstrated the flow and heat transfer over a tapered trapezoidal cylinder in both steady and periodic unsteady regimes (Re=1–150 and Pr=0.7). The onset of flow separation exists between Re=5 and 6, and the critical value of the Reynolds number (i.e., transition to time-periodic regime) exists between Re = 46 and 47. The drag coefficient decreases with increasing Re in the steady regime; however, the drag increases with Re in the periodic unsteady regime. The Strouhal number and the average Nusselt number increase with increasing Re. More recently, Dhiman et al. [16] numerically investigated effects of wall confinements on the laminar flow and heat transfer around a heated tapered trapezoidal bluff body in the confined domain for Re=1–40, blockage ratio = 0.125 –0.5, and Pr=0.71. They observed that the onset of flow separation is between Re=4 and 5 for the blockage ratio of 0.125 and between Re=5 and 6 for the blockage ratios of 0.25 and 0.5.

On the flow around an expanded trapezoidal cylinder, Lee [17] performed the 2-D numerical study of early stages of an impulsively started unsteady laminar flow past an expanded trapezoidal cylinder in which it is observed that the characteristics of the developing flow recirculation, flow separation and regimes caused by interacting of flows are strongly dependent on the approaching Reynolds number for the identical range of control parameters as in ref. [11]. The flow around a porous expanded trapezoidal cylinder using a finite volume method, based on the body-fitted, non-orthogonal grids and multi-block technique has been enumerated by Chen et al. [18]. The effects of the stress jump parameters (related to viscous and inertial effects) are

provided for Reynolds numbers of 20, 40, 100 and 200. Recently, Dhiman and Ghosh [19] simulated momentum and heat transfer phenomena across an expanded trapezoidal bluff body in both steady and unsteady regimes for identical range of settings as in ref. [15]. They observed that the wake length increases as Re increases in the steady flow regime ($1 \leq \mathrm{Re} \leq 47$). The transition from a steady to a periodic unsteady regime occurs between Re=47 and 48. The total drag coefficient decreases with increasing value of Re up to 90 and thereafter it increases with Re. However, heat transfer coefficient and Strouhal number increase with increasing Re.

Thus, based on the above discussion, it can be stated that although ample research works are available on the mixed convection flow across a square bluff body [20-23] but no work is currently available on flow around a trapezoidal bluff body even after trapezoidal body is reported to be the most suitable shape of bluff body for design of vortex flow meter. This work is hence intended to fill this gap in the literature and to investigate the mixed convection momentum and heat transfer across a trapezoidal bluff body for two configurations, namely tapered and expanded for the range of Reynolds number $10 \leq \mathrm{Re} \leq 50$, Richardson number $0 \leq \mathrm{Ri} \leq 1$ and for a fixed value of Prandtl number of 0.7 (air).

CHAPTER-3

PROBLEM DESCRIPTION AND NUMERICAL DETAILS

3.1 Problem statement

The 2-D, incompressible and laminar flow (flowing from left to right) across a long trapezoidal cylinder (long in neutral direction) is considered in an unconfined domain for two configurations: expanded (Fig. 2a) and tapered (Fig. 2b). At the inlet, the flow is uniform and isothermal with a velocity U_∞ and a temperature T_∞. The trapezoidal cylinder is maintained at a constant temperature of $T_w (> T_\infty)$. The dimensionless upstream distance from the inlet plane to the front surface of the trapezoidal cylinder X_u is set as 20 and the dimensionless downstream distance between the rear surface of the trapezoidal cylinder and the exit plane X_d is taken as 25, with the total dimensionless length of the computational domain (L) of 46 in the axial direction. The non-dimensional height of the computational domain (H) is used as 45 in the lateral direction. These distances are chosen after a thorough investigation and the details are provided in the section 3.3 titled "Numerical details."

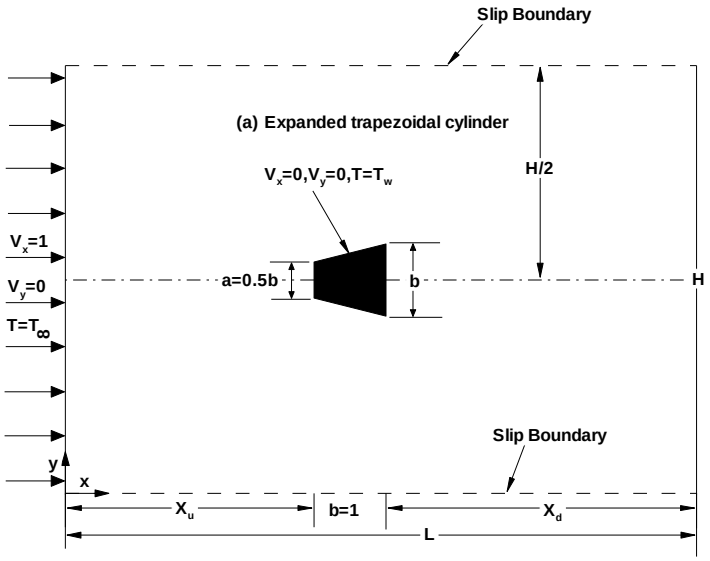

Figure 2(a): Schematics of flow and heat transfer across the expanded trapezoidal bluff body in an unconfined domain.

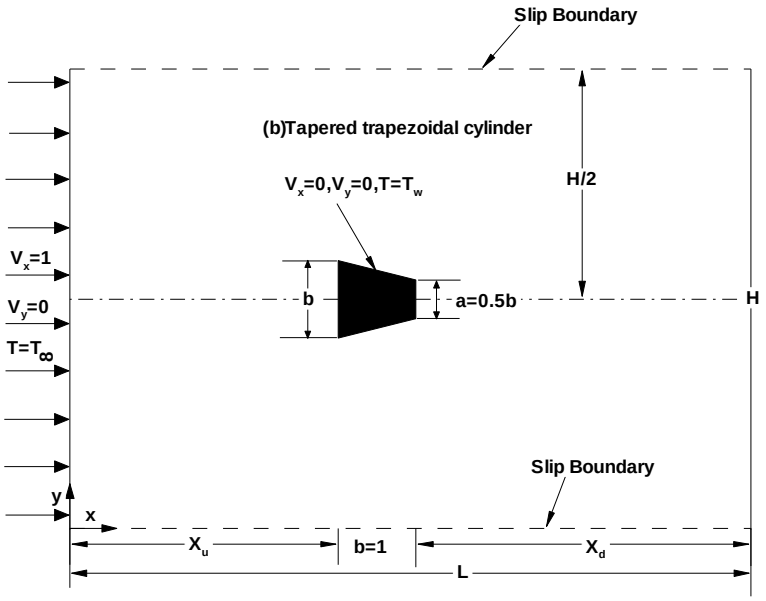

Figure 2(b): Non-uniform grid structure around the tapered trapezoidal bluff body in an unconfined domain.

3.2 Governing equations

The governing continuity, x- component and y- component of Navier-Stokes, and energy equations in their dimensionless form for the present system can be written as [24]:

Continuity equation

$$\frac{\partial V_x}{\partial x}+\frac{\partial V_y}{\partial y}=0 \tag{1}$$

x-Momentum equation

$$\frac{\partial V_x}{\partial t}+\frac{\partial (V_x V_x)}{\partial x}+\frac{\partial (V_y V_x)}{\partial y}=-\frac{\partial p}{\partial x}+\frac{1}{\mathrm{Re}}\left(\frac{\partial^2 V_x}{\partial x^2}+\frac{\partial^2 V_x}{\partial y^2}\right) \tag{2}$$

y-Momentum equation

$$\frac{\partial V_y}{\partial t}+\frac{\partial (V_x V_y)}{\partial x}+\frac{\partial (V_y V_y)}{\partial y}=-\frac{\partial p}{\partial y}+\frac{1}{\mathrm{Re}}\left(\frac{\partial^2 V_y}{\partial x^2}+\frac{\partial^2 V_y}{\partial y^2}\right)+\mathrm{Ri}\theta \qquad (3)$$

Energy equation

$$\frac{\partial \theta}{\partial t}+\frac{\partial (V_x \theta)}{\partial x}+\frac{\partial (V_y \theta)}{\partial y}=\frac{1}{\mathrm{Re}\,\mathrm{Pr}}\left(\frac{\partial^2 \theta}{\partial x^2}+\frac{\partial^2 \theta}{\partial y^2}\right) \qquad (4)$$

where Reynolds, Prandtl and Richardson numbers are defined as $\mathrm{Re}=bU_\infty \rho/\mu$ and $\mathrm{Pr}=\mu c_p/k$ and Ri= $g\beta(T_w-T_\infty)b/U_\infty^{\,2}$ respectively. In above equations (1-4), thermal and physical properties of fluid and bluff body are assumed to be constant with time and space. Variation of density has been incorporated in momentum conservation equation perpendicular to flow using boussinesq approximation.

The boundary conditions (in their dimensionless form) for the unconfined flow and heat transfer across a heated trapezoidal cylinder can be written as

- *At the inlet boundary,* $V_x=1$, $V_y=0$ and $\theta=0$
- *On upper and lower adiabatic boundaries,* $\partial V_x/\partial y=0$, $V_y=0$ and $\partial\theta/\partial y=0$
- *On the surface of the trapezoidal obstacle,* $V_x=0$, $V_y=0$ and $\theta=1$
- *At the exit boundary,* $\partial V_x/\partial x=0; \partial V_y/\partial x=0$ and $\partial\theta/\partial x=0$

3.3 Numerical details

The governing equations (1 - 4) along with above noted boundary conditions are solved by using a finite volume solver Ansys [25]. The second order upwind scheme is used to discretize convective terms; whereas, the diffusive terms are discretized by central difference scheme. The resulting algebraic equations are solved by Gauss-Siedel iterative scheme in conjunction with Algebraic Multi-Grid solver. The absolute residuals of the continuity, x- and y-velocities and energy are used of the order of 10^{-10} each in the steady regime and of the order of 10^{-20} each in the unsteady regime. The second order implicit time-integration method is used and

the dimensionless time step is set to 0.01 [15,19]. To determine the optimum value of the time step, two values of the time step (0.01 and 0.005) were studied at Re=50 and Ri=1. For the expanded body, percentage deviation in total drag coefficient is found to be less than 0.5%, while deviation in Nusselt number is found to be less than 0.1% and deviation in Strouhal number is found to be about 1.4%. The corresponding deviations for the case of a tapered trapezoidal body are found to be about 0.90%, 0.30% and 1.9%. Since the maximum deviation is found to be insignificant when step size is reduced so 0.01 is considered as time step in evaluating the results.

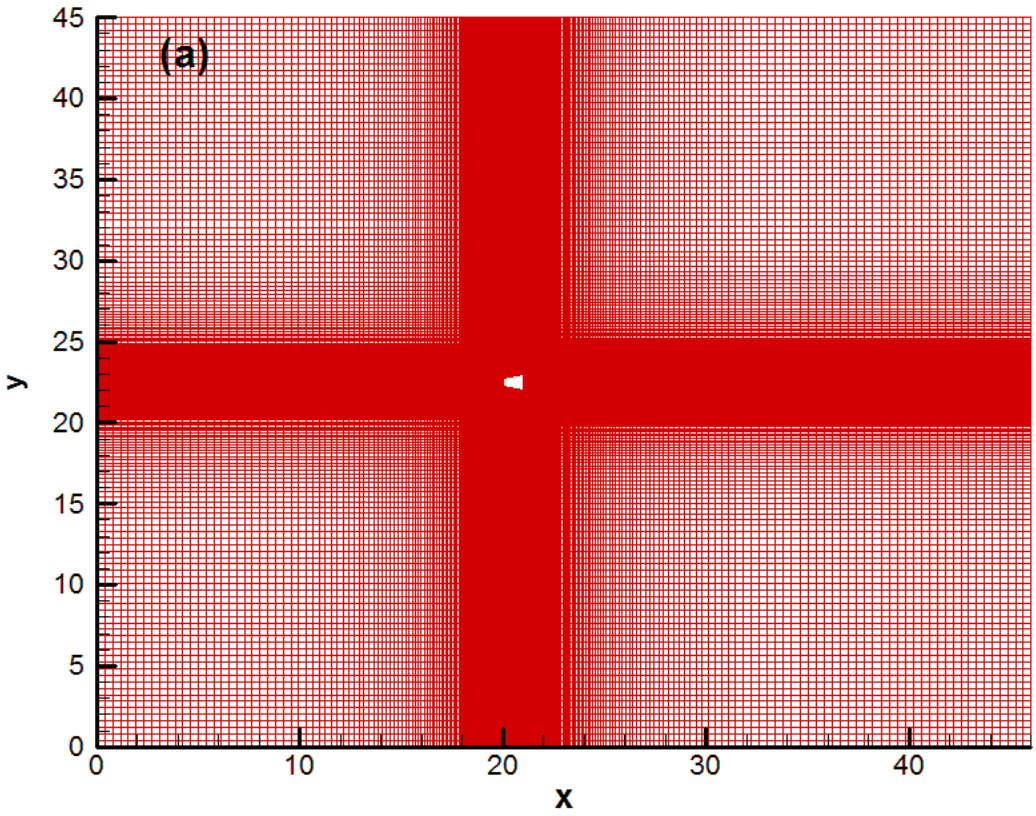

Figure 3(a): Non-uniform grid structure around the expanded trapezoidal bluff body in an unconfined domain.

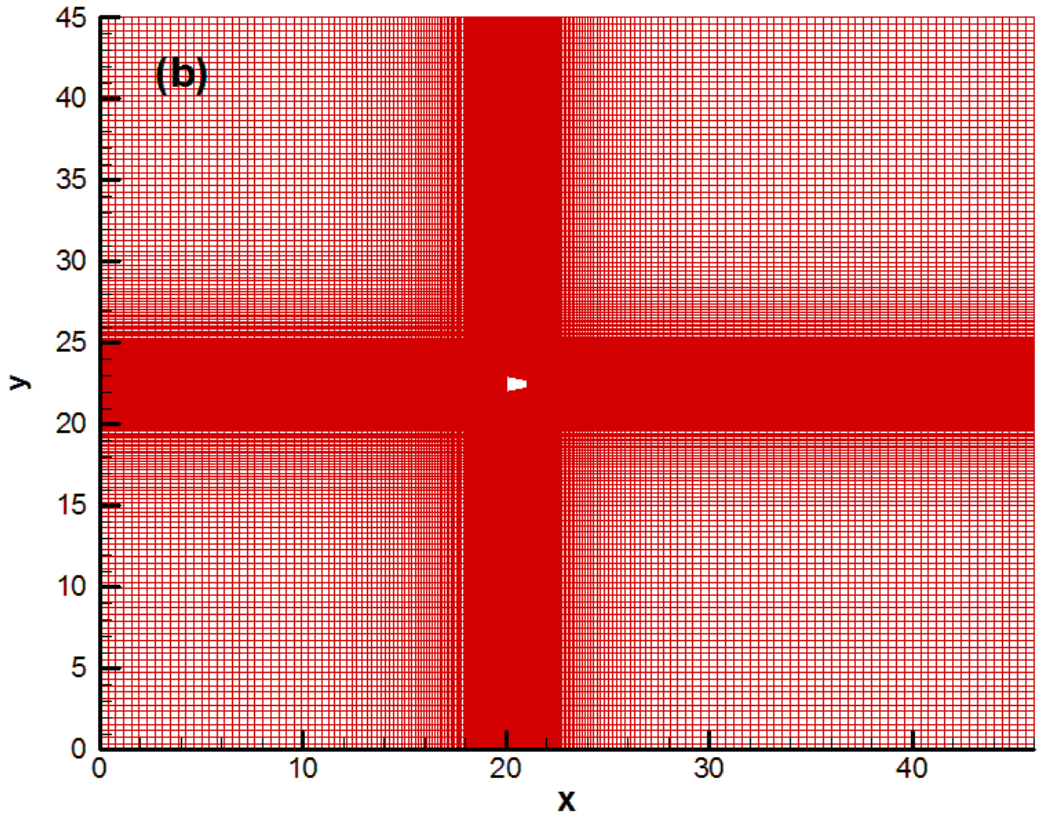

Figure 3(b): Non-uniform grid structure around the tapered trapezoidal bluff body in an unconfined domain.

The computational grid structure which has been used for the simulation generated by using Ansys [25], as shown in Figs. 3(a, b). For selection of grid in case of the tapered obstacle, two non-uniform grids with 147608 and 162458 quadrilateral cells having 100 and 125 control volumes (CVs) were simulated at Re=50, Ri=1 and Pr=0.7. The percentage deviation in total drag coefficient, Nusselt and Strouhal numbers was found to be about 0.85%, 0.35% and 1.8% respectively. Also, for the expanded body, two different grids with 148950 and 163225 cells were chosen, containing 100 and 125 CVs respectively. The percentage deviation of about 0.4% was obtained in total drag coefficient, while the deviation in Nusselt and Strouhal numbers was obtained about 0.05% and 1.35% respectively. Hence, for both the geometries, it can be seen that deviation is not much prominent as we moved to a larger grid. Hence, the grids with 100 CVs prescribed on the surface of the bluff body are selected for both expanded and tapered

geometries. The dimensionless grid spacing has been taken to be as fine as 0.004 near the the bluff body which goes up to the highest value of 0.4 away from the obstacle for expanded as well as tapered [15,19].

To carry out the upstream distance independence test, two different values of upstream distances of 20 and 25 have been simulated at Re=10, Ri=1 and Pr=0.7 for both the geometries. In case of the tapered body, percentage deviations in the values of total drag coefficient, average cylinder Nusselt and Strouhal numbers were about 0.7%, 0.1% and 1.25% respectively, and the corresponding percentage deviations for the expanded geometry were about 0.1%, 0.07% and 0.2%. Hence, the dimensionless upstream distance was fixed as 20 to carry out further calculations as by increasing the upstream distance further the results changed marginally.

Similarly, the downstream distance of both geometries have been fixed by taking two values of dimensionless downstream distances of 25 and 30 and simulating at Re=50, Ri=1 and Pr=0.7. In case of the tapered body, the percentage deviation in total drag coeffiecient, Nusselt and Strouhal numbers was obtained about 0.2%, 0.02% and 0.5% respectively, while for the expanded geometry the corresponding deviation was about 0.3%, 0.04% and negligibly small. Therefore, the dimensionless downstream distance of 25 is found sufficient for the generation of results.

Ultimately, the height of the computational domain has been chosen by varying the value of the domain height from 45 to 50 and simulating at Re=50, Ri=1 and Pr=0.7. While the percentage deviations in the values of the total drag coefficient, average cylinder Nusselt number and Strouhal number were found to be about 0.25%, 0.01% and 0.25% respectively for the tapered body. The corresponding percentage deviations were about 0.5%, 0.05% and 0.3% in case of the expanded geometry. Thus, the dimensionless height of the computational domain of 40 is used here. Hence to sum up, the following numerical parameters have been chosen from above mentioned independence studies: Time step=0.01, Control volume=100, X_u=20, X_d=25 and H=45.

Table 1: Time independence test for expanded and tapered geometries at Ri=1, Re=50.

Expanded(Ri=1,Re=50)					Tapered(Ri=1,Re=50)				
Time step	C_D	C_L	St	Nu	Time step	C_D	C_L	St	Nu
ΔT=0.01	0.962	-2.201	0.133	3.697	ΔT=0.01	1.579	-0.864	0.121	2.896
ΔT=0.005	0.967	-2.208	0.135	3.699	ΔT=0.005	1.566	-0.869	0.124	2.888
%Deviation	0.46	0.35	1.39	0.06	%Deviation	0.85	0.54	1.88	0.28

Table 2: Grid independence test for expanded and tapered geometries at Ri=1, Re=50.

Expanded(Ri=1,Re=50)					Tapered(Ri=1,Re=50)				
CV	C_D	C_L	St	Nu	CV	C_D	C_L	St	Nu
100	0.963	-2.200	0.133	3.697	100	1.579	-0.864	0.121	2.896
125	0.966	-2.201	0.131	3.699	125	1.593	-0.865	0.119	2.906
%Deviation	0.37	0.02	1.33	0.05	%Deviation	0.84	0.04	1.80	0.33

Table 3: Upstream independence test for expanded and tapered geometries at Ri=1, Re=10.

Expanded(Ri=1,Re=10)					Tapered(Ri=1,Re=10)				
Domain	C_D	C_L	St	Nu	Domain	C_D	C_L	St	Nu
Xu=20,Xd=25, H=45	1.079	-2.757	0.023	1.684	Xu=20,Xd=25 ,H=45	1.526	-2.040	0.041	1.451
Xu=25,Xd=25, H=45	1.078	-2.757	0.022	1.683	Xu=25,Xd=25 ,H=45	1.536	-2.056	0.042	1.453
%Deviation	0.12	0	0.22	0.07	%Deviation	0.70	0.79	1.25	0.11

Table 4: Downstream independence test for expanded and tapered geometries at Ri=1, Re=50.

Expanded(Ri=1,Re=50)					Tapered(Ri=1,Re=50)				
Domain	C_D	C_L	St	Nu	Domain	C_D	C_L	St	Nu
Xu=20,Xd=25, H=45	0.962	-2.201	0.133	3.697	Xu=20,Xd=25 ,H=45	1.579	-0.864	0.121	2.896
Xu=20,Xd=30, H=45	0.965	-2.203	0.133	3.698	Xu=20,Xd=30 ,H=45	1.582	-0.866	0.122	2.897
%Deviation	0.29	0.12	0	0.04	%Deviation	0.18	0.25	0.48	0.02

Table 5: Height independence test for expanded and tapered geometries at Ri=1, Re=50.

Expanded(Ri=1,Re=50)					Tapered(Ri=1,Re=50)				
Domain	C_D	C_L	St	Nu	Domain	C_D	C_L	St	Nu
Xu=20,Xd=25, H=45	0.962	-2.201	0.133	3.697	Xu=20,Xd=25 ,H=45	1.579	-0.864	0.121	2.896
Xu=20,Xd=25, H=50	0.957	-2.200	0.132	3.695	Xu=20,Xd=30 ,H=45	1.575	-0.862	0.122	2.897
%Deviation	0.50	0.01	0.26	0.05	%Deviation	0.25	0.20	0.24	0.01

CHAPTER 4

RESULTS AND DISCUSSIONS

In the current study, air has been considered as the working fluid. The 2-D numerical simulations have been performed to examine and analyze the laminar mixed convection flow and heat transfer across (heated) expanded and tapered trapezoidal bluff bodies in an unconfined domain. The results have been generated for the range of control parameters as: Re=10–50 (in the interval of 10), Ri=0, 0.5 and 1.0 and Pr=0.7. A comparison has been made between the two geometries, to understand the effect of shape on the flow and thermal phenomena under cross-buoyancy.

The dimensionless output parameters such as drag and lift coefficients, local and average Nusselt numbers are calculated. Streamline and isotherm contours are added to comprehend the flow and thermal patterns respectively around the tapered and expanded cylinders. In the end, an empirical correlation has been provided to calculate the average Nusselt number for the preceding range of settings.

4.1 Validation of results

Extensive benchmarking has been done to justify the appropriateness of the numerical method used here to obtain the reliable results. The present results are benchmarked using results of Dhiman and Ghosh [19] for an expanded body at Ri=0 and Re=10-50. Fig. 4 shows the comparison of results obtained by Dhiman and Ghosh [19] and in present work. An excellent agreement is found between the two studies.

Similarly, for a tapered trapezoidal body, the results obtained for Ri=0, Re=10-50 and these were compared with the results of Dhiman and Hasan [15]. Fig. 5 shows the comparison of results of Dhiman and Hasan [15] and present work. Again, it can be seen that an excellent agreement exists between the works.

The present numerical methodology is further validated with the results of Chung and Kang [12] for air flow around a tapered trapezoidal body for Re=100 and 150 at Ri=0. Chung and Kang [12] reported Strouhal numbers to be 0.138 and 0.149 for Re=100 and 150 respectively. While with present methodology, the Strouhal numbers obtained at same operating

conditions are 0.135 and 0.144 for Re=100 and 150 respectively. Hence, an excellent agreement can be seen between the results presented in ref. [12] and the present work, and hence the current numerical methodology can be used to generate further results.

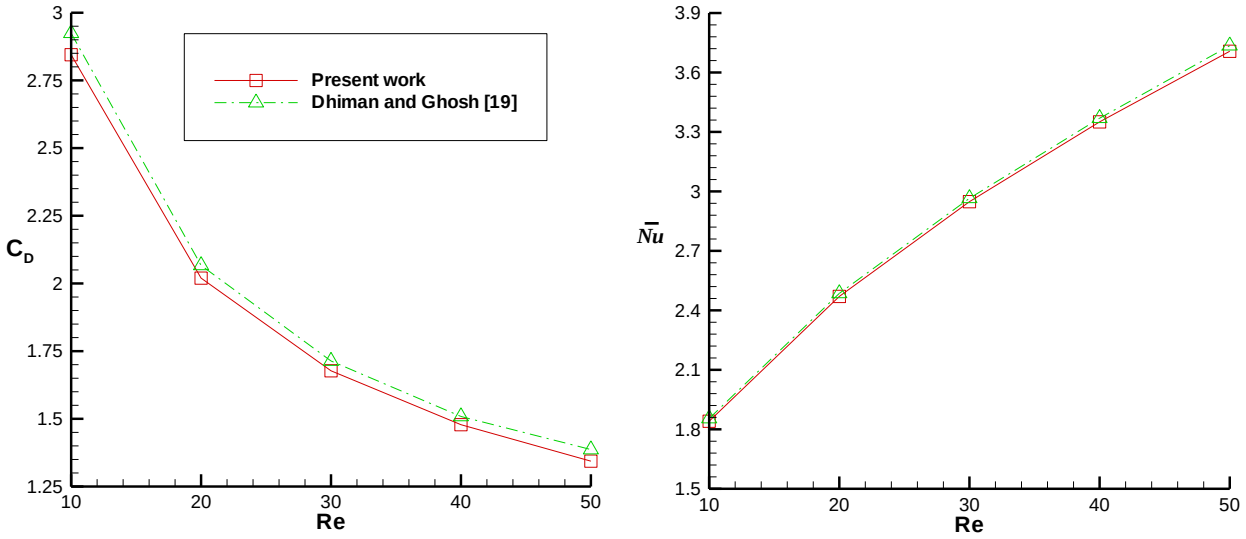

Figure 4: Comparison of C_D and $\bar{Nu}$ results of Dhiman and Ghosh [19] with present work.

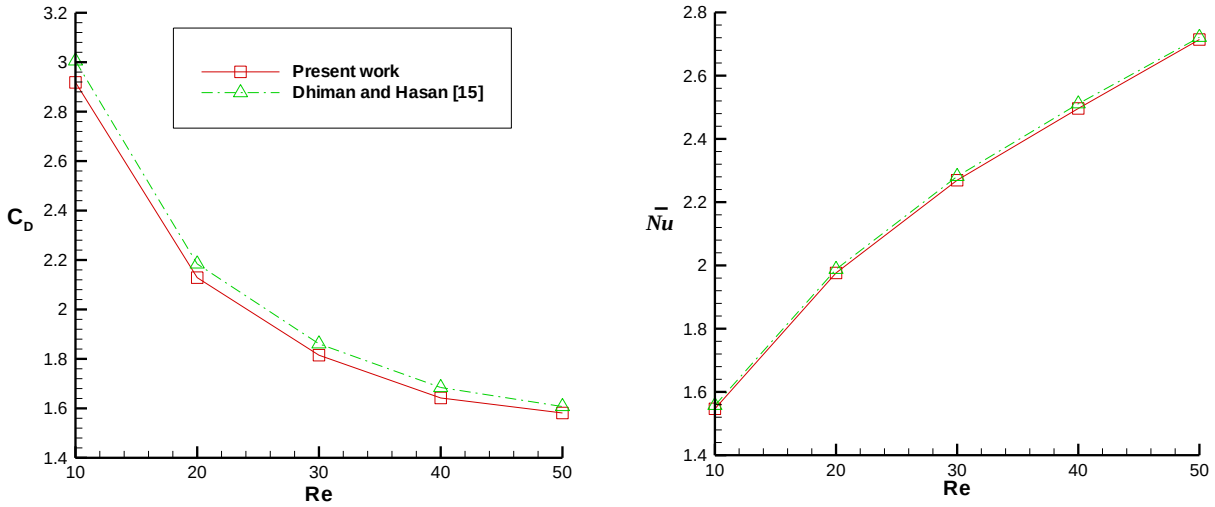

Figure 5: Comparison of C_D and $\bar{Nu}$ results of Dhiman and Hasan [15] with present work.

4.2 Flow patterns

The flow patterns have been represented through streamline contours, which give indication of type of flow whether steady or unsteady and also tell about flow separation from the body. As mentioned by Dhiman and Ghosh [19], transition from a steady to a time-periodic regime (critical Re) for the expanded geometry was found to be between Re=47 and 48 at Ri=0 (forced convection). It has been observed that critical Reynolds number decreases with increase in Ri. At Ri=0.5, critical Re was obtained between Re=46 and 47. A comparison of flow and thermal patterns and time history of lift coefficient at critical Reynolds number for the expanded geometry at Ri=0.5 is given in Fig. 6.

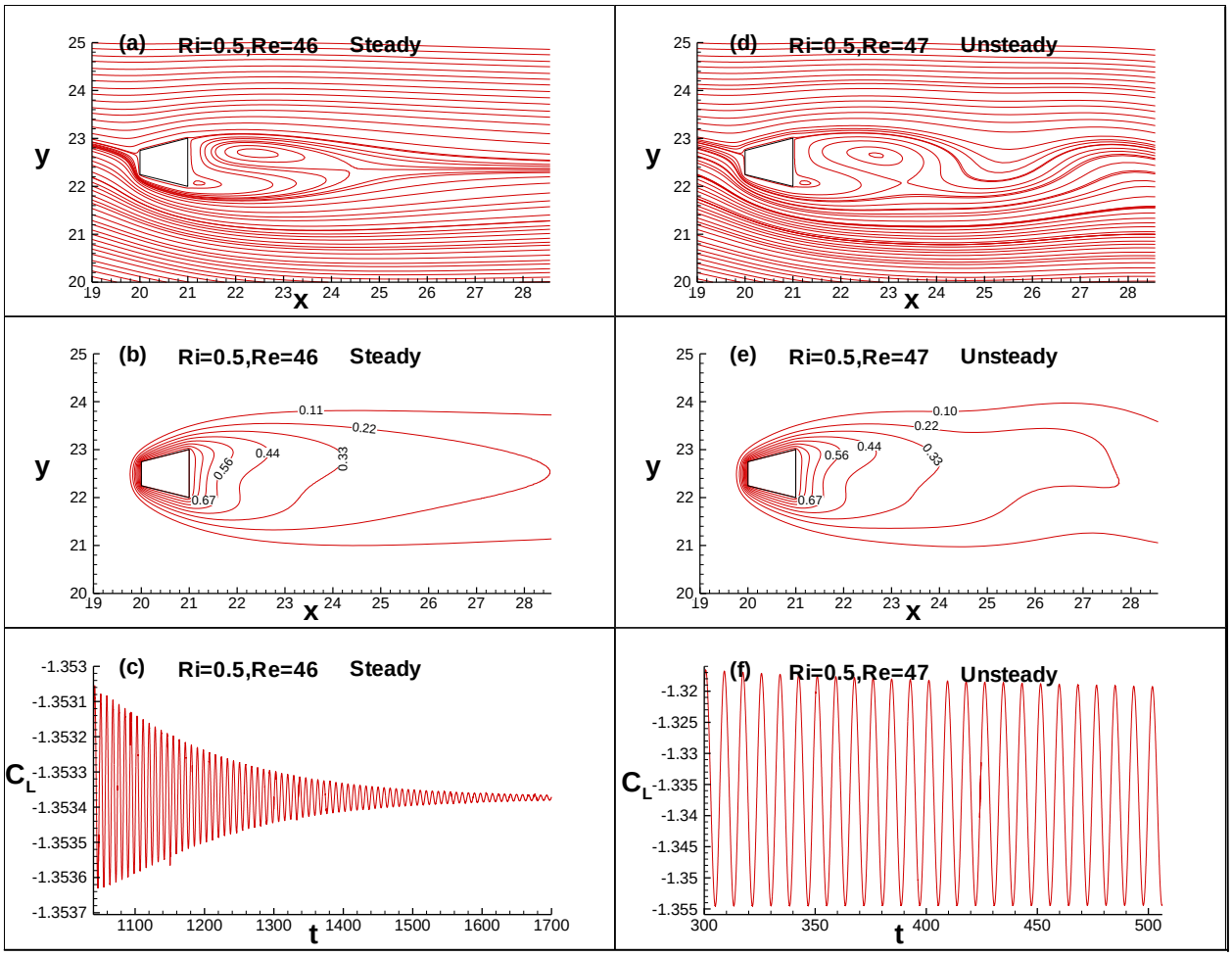

Figure 6: Streamlines, isotherms and lift coefficient showing transition from steady to time-periodic regime for an expanded bluff body.

Similarly, the observation of Dhiman and Hasan [15] about critical Re for a tapered body in case of Ri=0 was confirmed to be between Re=46 and 47. At Ri=0.5, critical Re for the tapered geometry was found to be between Re=35 and 36, and comparison of flow and thermal patterns and time history of lift coefficient at Ri=0.5 for the tapered geometry is given in Fig. 7.

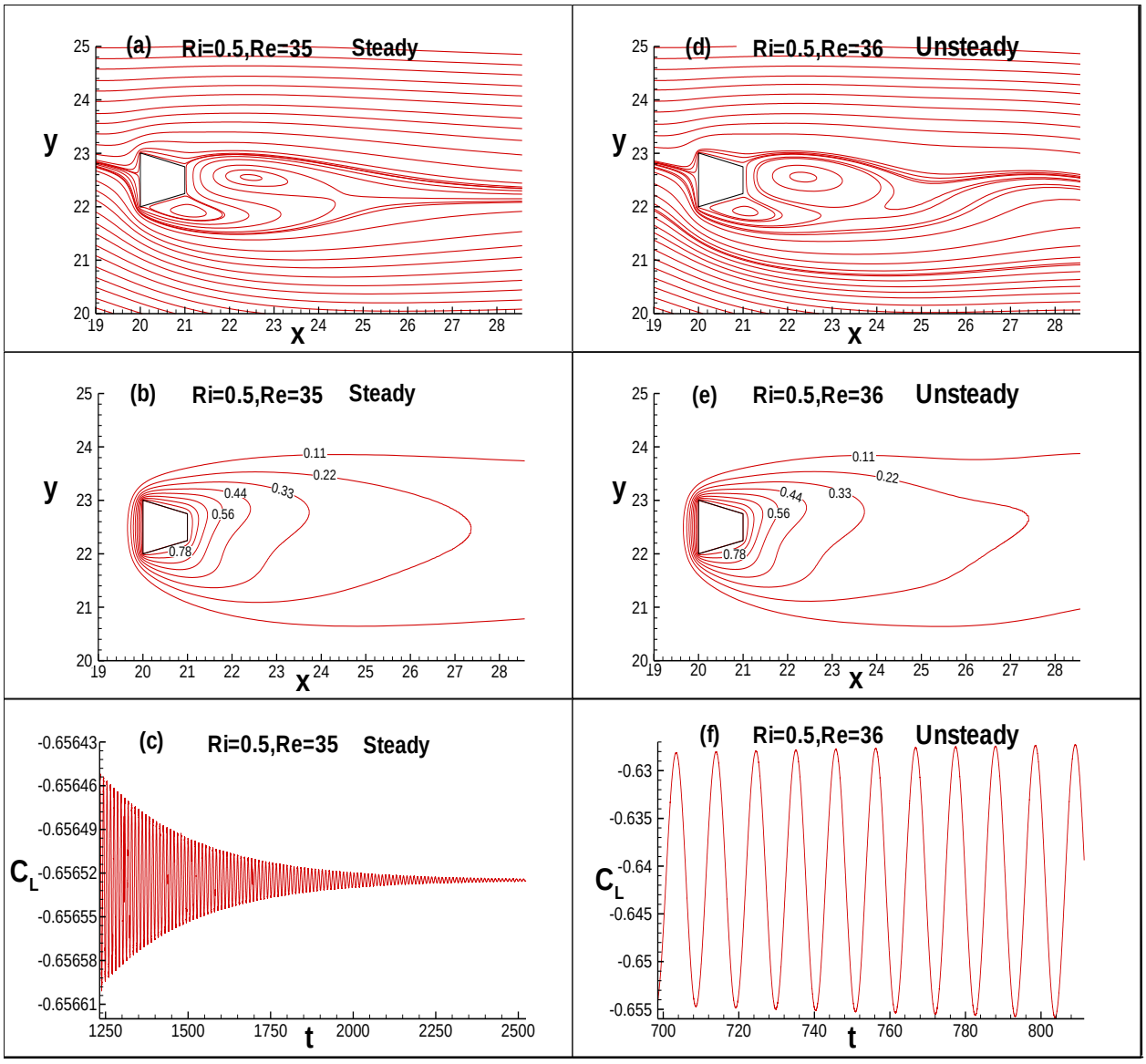

Figure 7: Streamlines, isotherms and lift coefficient showing transition from steady to time-periodic regime for the tapered bluff body.

It can also be observed that critical Re decreases as one move from expanded to tapered bluff body for a fixed value of Ri because of the more blunt nature of the later body. Also critical Re is found to decrease with increase in Ri for both the geometries because increasing Ri leads to increase in periodic flow and hence leads to decrease in critical Re. The critical Re for Ri=1 is observed to be less than Re=10 for both the bluff bodies. However, exact evaluation of critical Re at Ri=1 is not accomplished here because of extensive domain requirement to delineate accurate results at low Re. Nature of flow (steady or time-periodic unsteady) at various operating conditions is mentioned in Table 6 so as to give a quick insight of flow behavior at a given operating conditions.

Table 6: Nature of flow patterns: steady (S) and time-periodic (US) regimes.

Re	Ri=0		Ri=0.5		Ri=1	
	Expanded	Tapered	Expanded	Tapered	Expanded	Tapered
10	S	S	S	S	US	US
20	S	S	S	S	US	US
30	S	S	S	S	US	US
40	S	S	S	US	US	US
50	US	US	US	US	US	US

For comparison of flow patterns for the two trapezoidal bluff bodies, streamlines at two extreme values of Re=10 and 40 have been given in Figs. 8 and 9 respectively. At Re=10, one can notice that for Ri=0 the streamlines are symmetric about the centerline but as we increase Richardson number then effect of cross-buoyancy comes into play and flow becomes asymmetric. Also with increased cross-buoyancy, flow becomes time-periodic even at low Re of 10 (Figs. 8c, 8f). Since the expanded body is more streamlined as compared to the tapered trapezoidal body, flow separation in the expanded body is at rear end while in the tapered body

flow separation occurs even from top or bottom inclined edge of cylinder. At a given Re as we increase the effect of cross-buoyancy flow separation starts earlier and flow tends to become more periodic. Also wake region is larger in the expanded trapezoidal cylinder as compared to the tapered trapezoidal cylinder.

For a constant Ri as we increase Re wake region increases continuously and also the tendency of periodic flow assents causing the frequency and hence Strouhal number increases. More information on the effect of Strouhal number with Re is mentioned in section 4.6. As we increase Re, eddies formation become much more prominent because of increased dominance of inertial forces as compared to viscous forces leading to high tendency of vortex formation. Flow separation also begins earlier on advancing Re for expanded as well as tapered geometries. At Re=40 and Ri=0, the eddies are not fluctuating for both expanded and tapered bluff bodies and hence this operating condition represents steady flow for both the geometries (Figs. 9a, 9d). At Ri=0.5 and Re=40, for the expanded bluff body one of the eddies just behind the body is suppressed due to asymmetric nature of flow leading to difference in length of vortices formed but these vortices are also not fluctuating and hence represents steady flow. On the contrary for the tapered bluff body at same condition, flow has become periodic unsteady as critical Reynolds number of tapered bluff body at Ri=0.5 is obtained earlier than expanded body. For Ri=1, the flow is periodic unsteady for both the geometries for the range of Reynolds number considered in this study. Thus for Ri=1, critical Reynolds number would be less than Re=10 for both expanded as well as tapered trapezoidal cylinder.

Furthermore, streamlines at different times (T_p, T_p /4, T_p /2 and $3T_p/4$) in periodic unsteady state are provided at Re=50 in Figs. 10 and 11 for Ri=0.5 and 1 respectively and streamlines at Ri=0 is provided in [15, 19]. Vortices formed here fluctuate and after time period equals to T_p it repeats itself. The frequency of fluctuation gives the Strouhal number and represents the oscillatory nature of flow. It can be observed from the streamlines that in case of tapered geometry vortices are formed beneath the bottom surface of tapered body. This phenomena cause heat transfer from the bottom surface of tapered body to aggrandize and also lift coefficient increases.

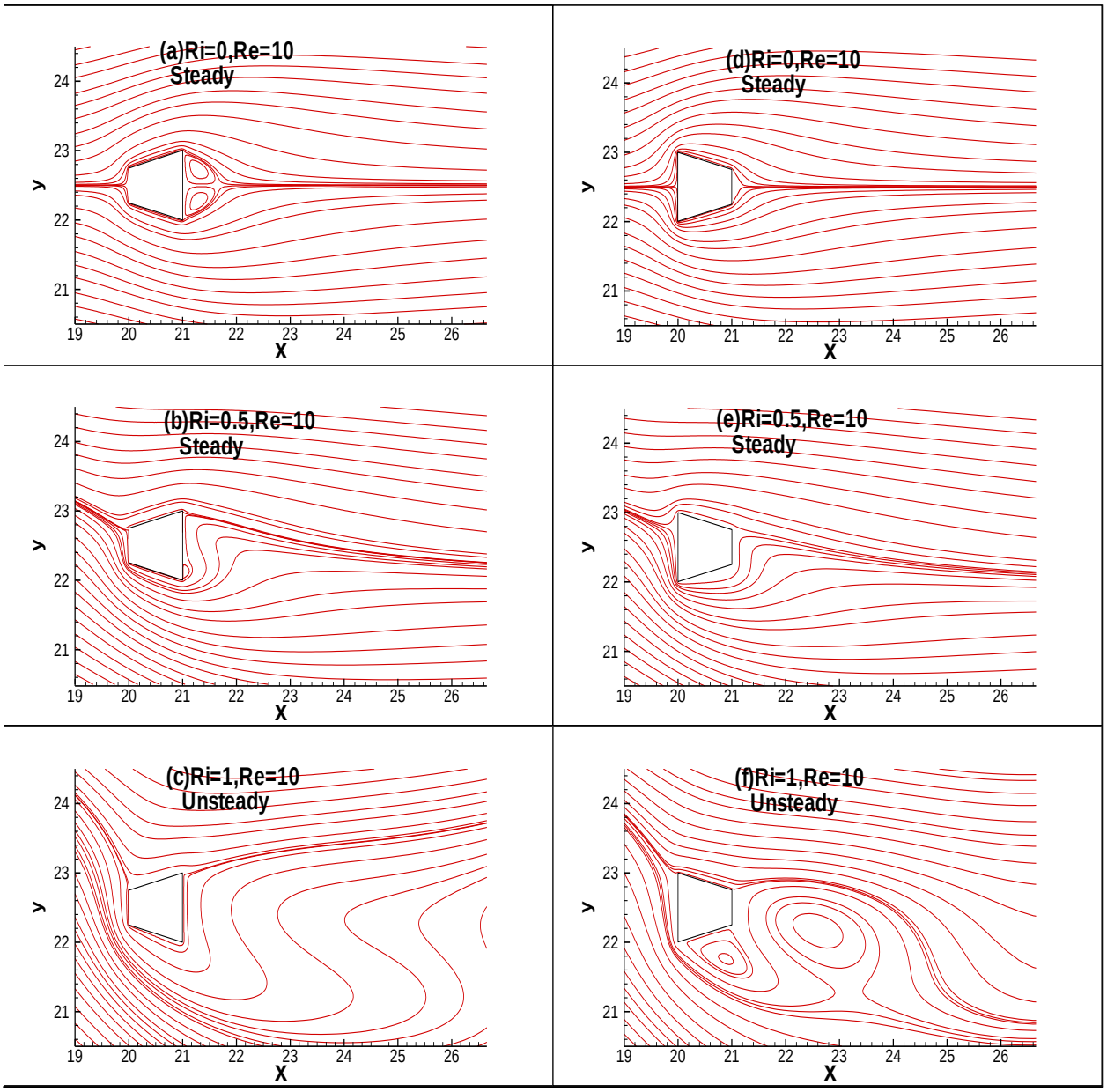

Figure 8: Streamlines at Re=10 for (a-c)expanded and (d-f)tapered trapezoidal cylinders at different Ri.

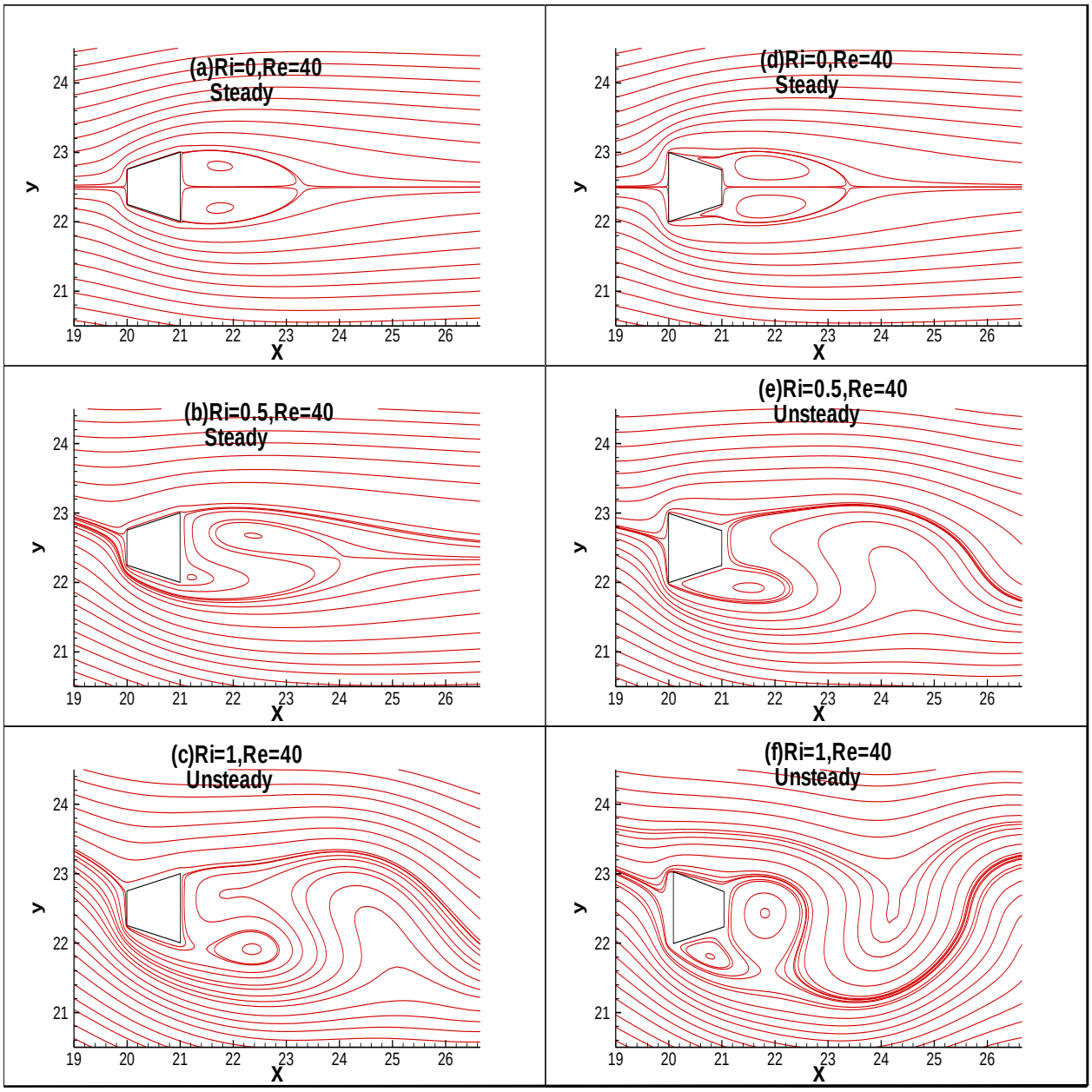

Figure 9: Streamlines at Re=40 for (a-c)expanded and (d-f)tapered trapezoidal cylinders at different Ri.

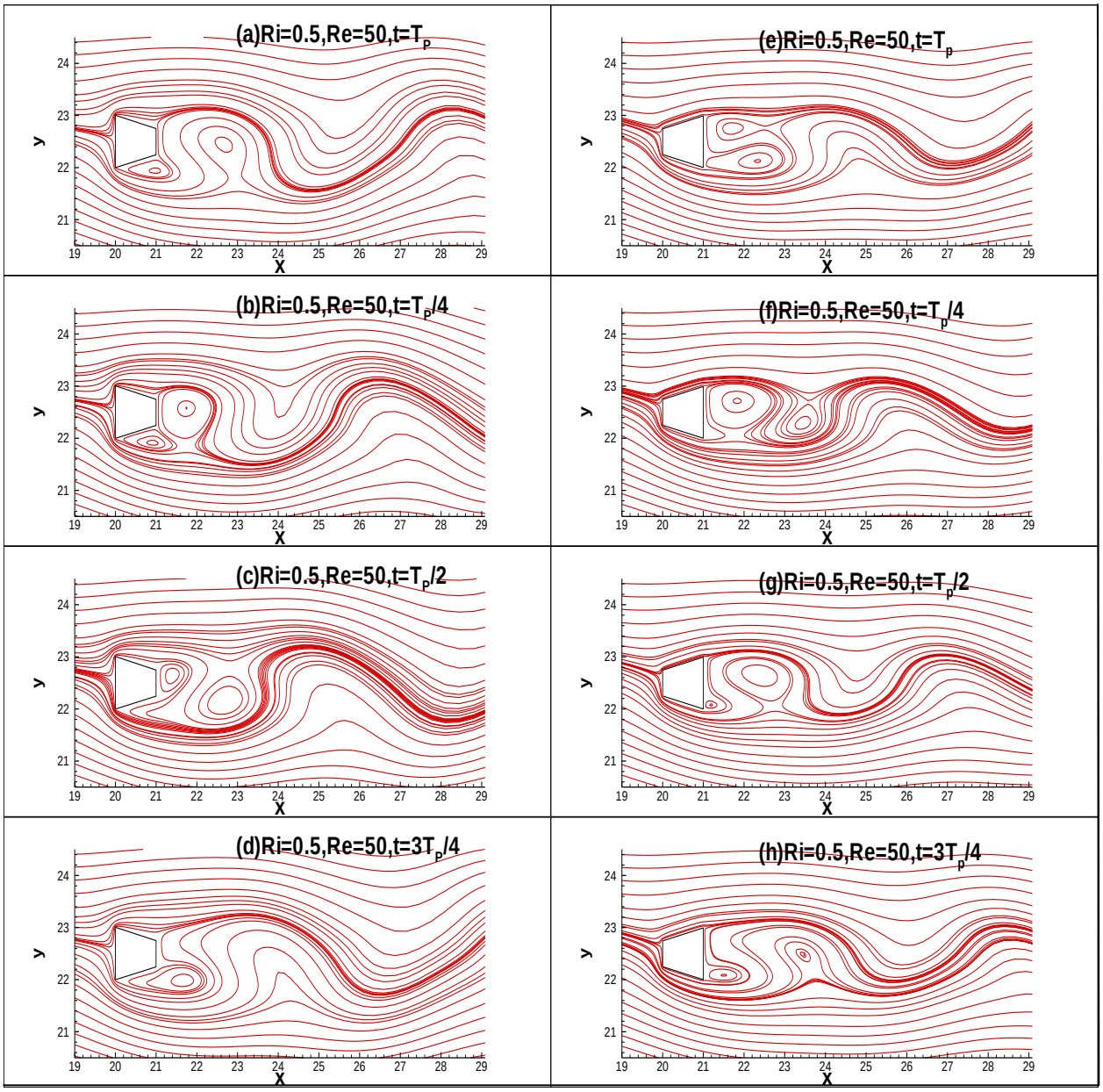

Figure 10: Streamlines for (a-d)tapered and (e-h)expanded cylinders at Ri=0.5 and Re=50 in periodic unsteady regime.

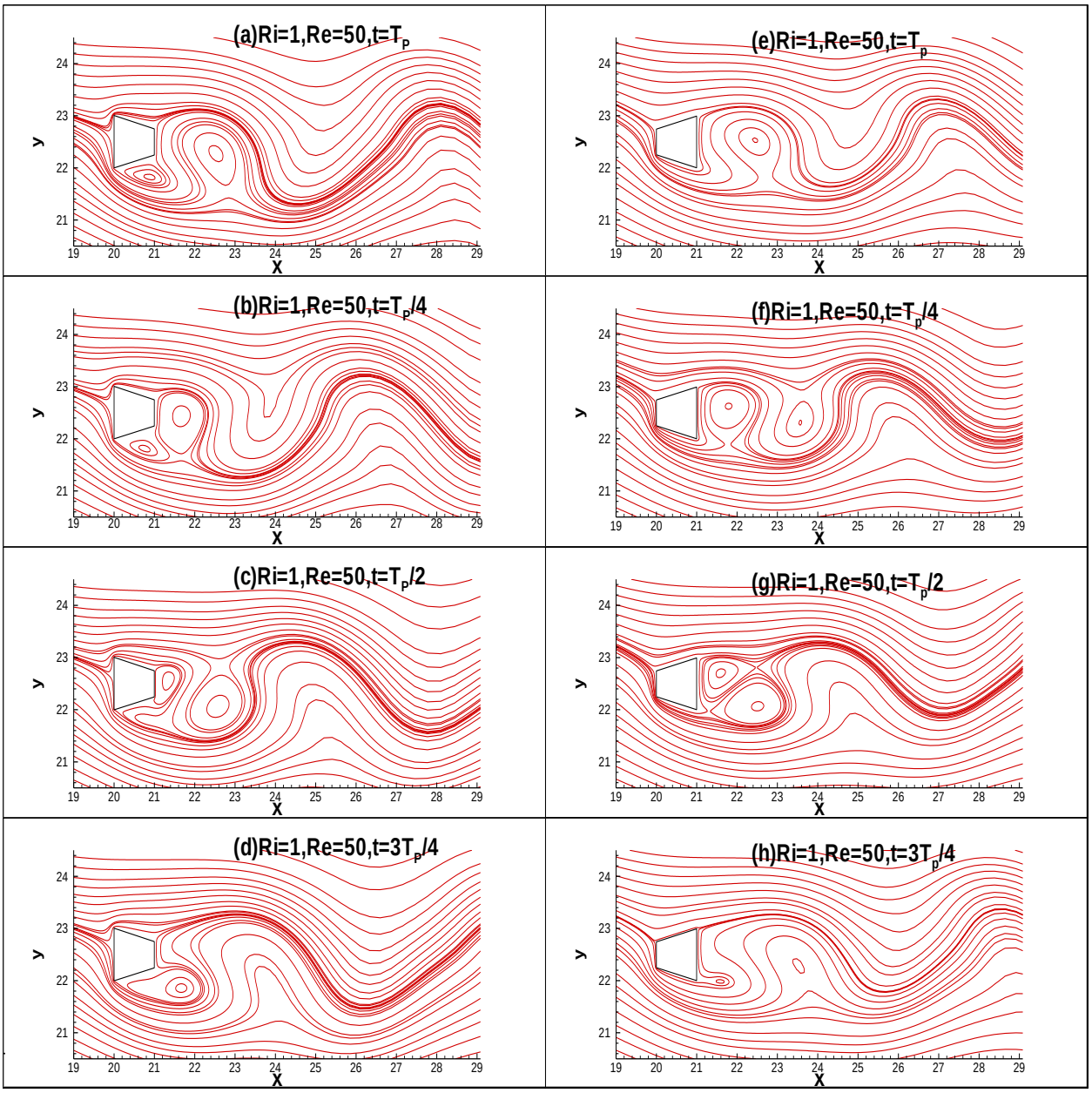

Figure 11: Streamlines for (a-d)tapered and (e-h)expanded cylinders at Ri=1 and Re=50 in periodic unsteady regime.

4.3 Thermal patterns

Isotherm contours are lines of constant temperature, and gives information about heat transfer rate. If the contours are rounded in shape, then it signifies that an appreciable amount of heat transfer has occurred as now the effect of heated cylinder can be seen even farther away from cylinder. On the contrary for flat isotherm contours, heat transfer is not that much effective as compared to heat transfer in a rounded shape of isotherm contour.

For comparison of thermal patterns at steady and periodic unsteady states, isotherm contours are provided for both the trapezoidal cylinders at extreme values of Re (10, 40) for different Ri in Figs. 12 and 13. For steady regime and neutral buoyancy (Ri=0), the contours are rounded in shape and are symmetric, but as the effect of cross-buoyancy (Ri) is induced isotherms become asymmetric about the centerline. With increase of Re isotherms tend to elongate as depicted in figures. Elongation of isotherm represents dominance of inertial forces as compared to viscous forces. On comparing isotherms for expanded and tapered geometries at same operating conditions, it is found that for the expanded body isotherms are more elongated as compared to the tapered one. This is due to the streamline nature of expanded body. In time-periodic regime, isotherms are not constant and oscillate with time in a similar manner as observed in Figs. 10 and 11. Isotherms at Re=50 for Ri=0.5 and 1 is given in Figs. 14 and 15 respectively. Time-periodic isotherms for Ri=0 and Re=50 is provided in [15, 19]. Fluctuation in isotherm contour suggests oscillating heat transfer rate. More information on variation of Nu with Re and Ri is mentioned in section 4.7. On increasing Ri keeping other factors constant we can observe an increase in wake region because of increase in heat transfer rate caused due to increase in periodic nature of flow. The numbers marked on isotherm contours are the dimensionless temperature at that contour. The value of this dimensionless temperature is close to 1 near the cylindrical surface and approaches 0 far from the body.

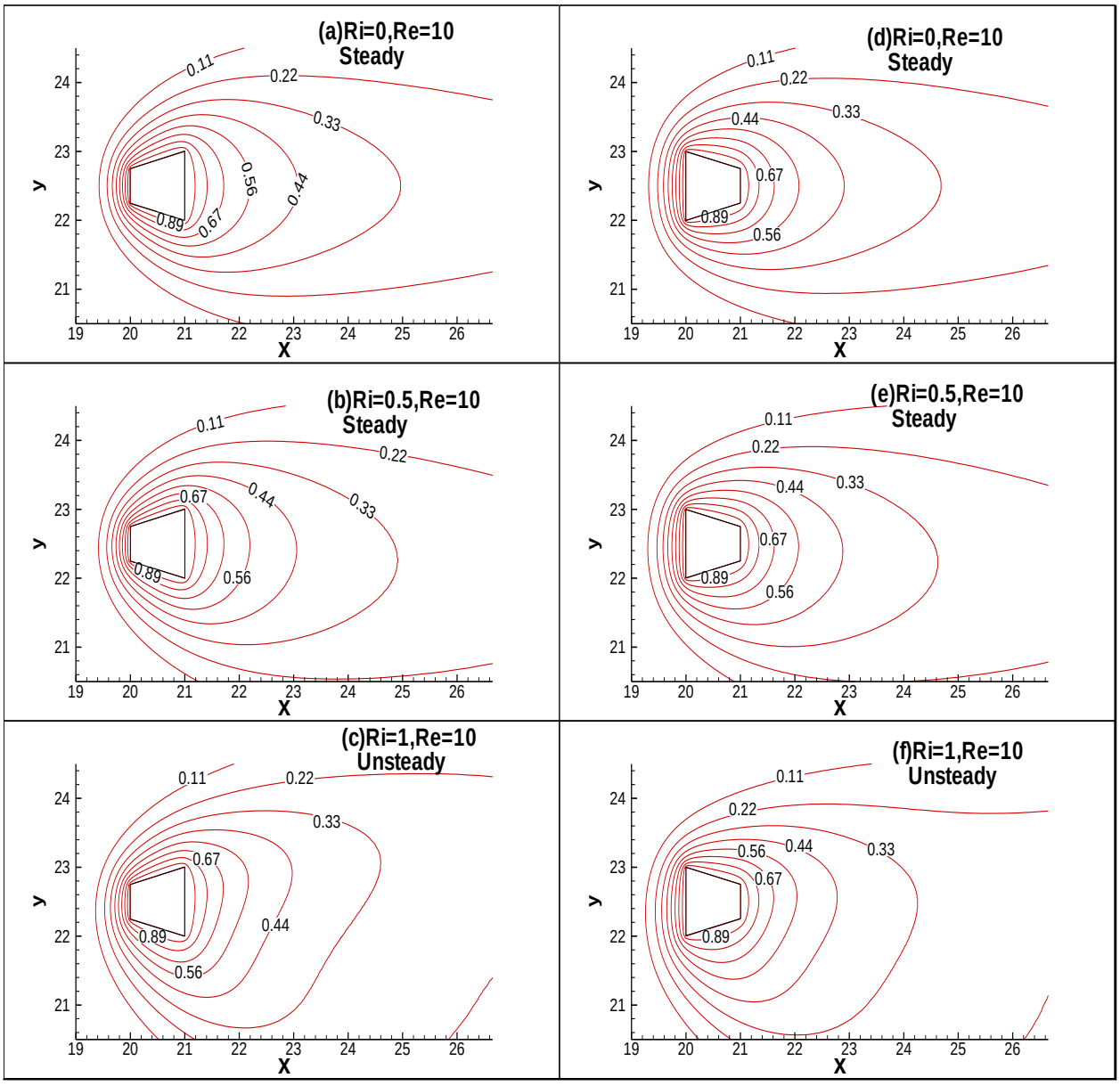

Figure 12: Isotherms for (a-c)expanded and (d-f)tapered trapezoidal cylinders for Re=10 at different Ri.

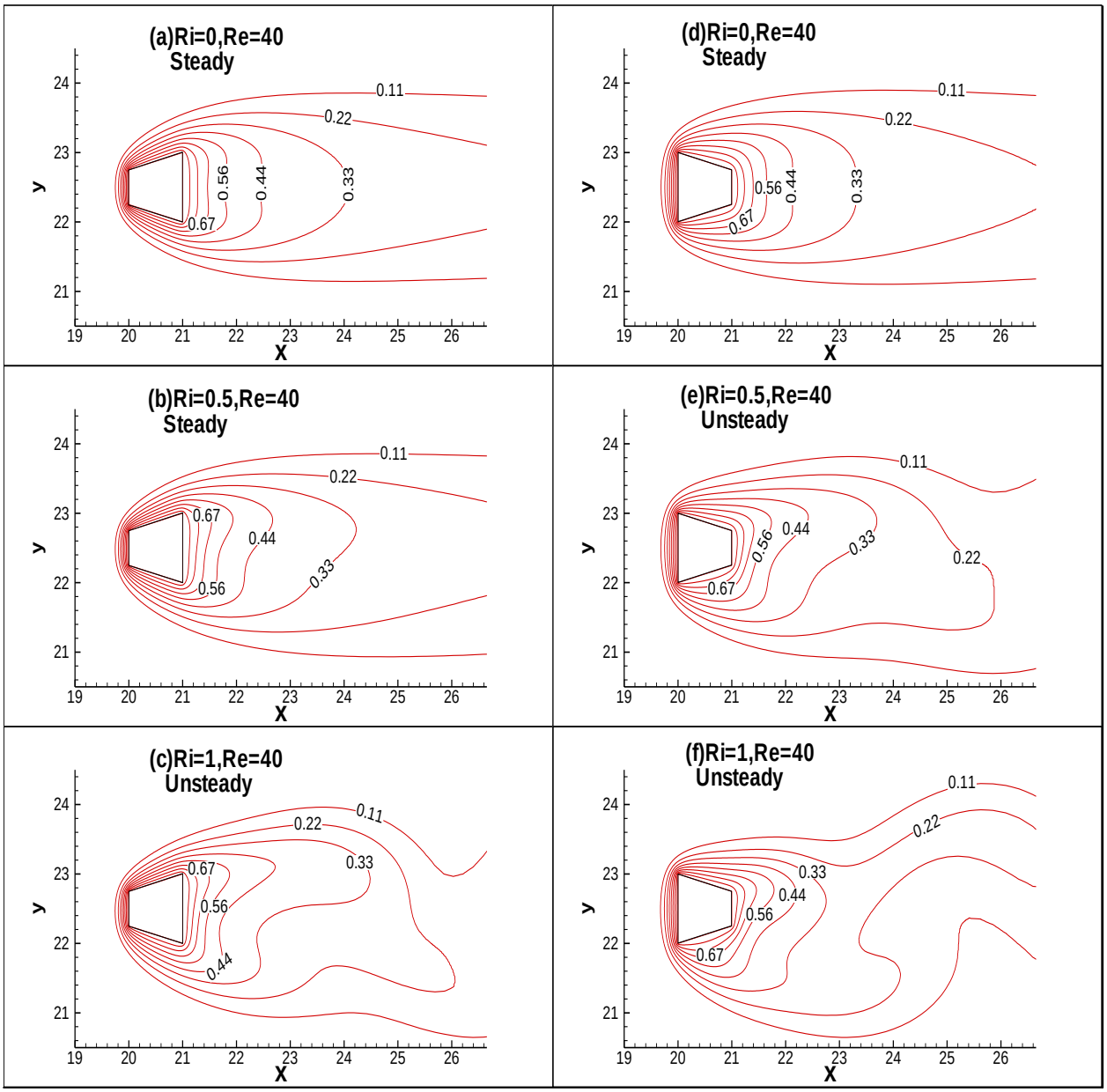

Figure 13: Isotherms for (a-c)expanded and (d-f)tapered trapezoidal cylinders for Re=40 at different Ri.

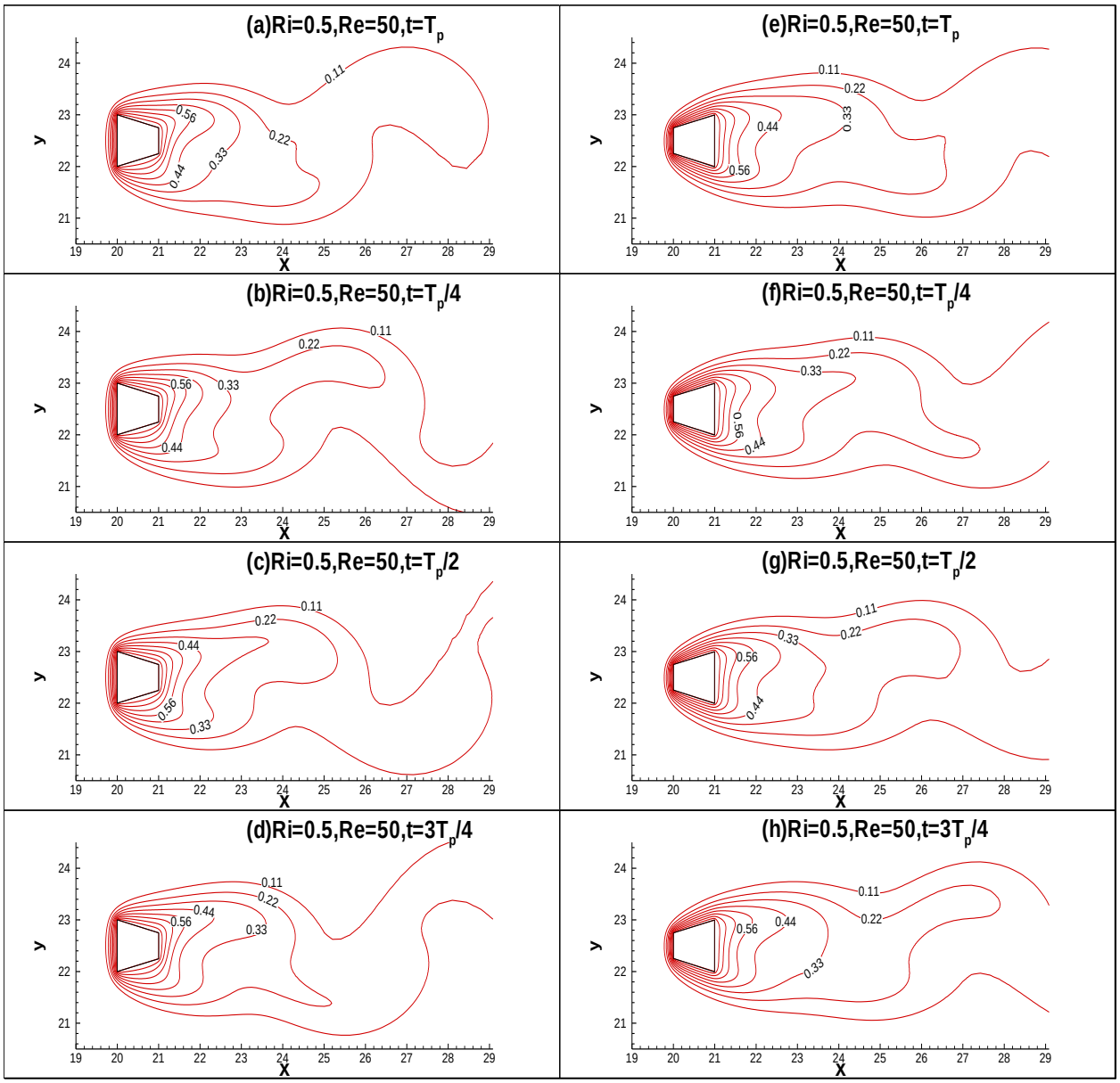

Figure 14: Isotherms for (a-d)tapered and (e-h)expanded cylinders at Ri=0.5 and Re=50 in periodic unsteady regime.

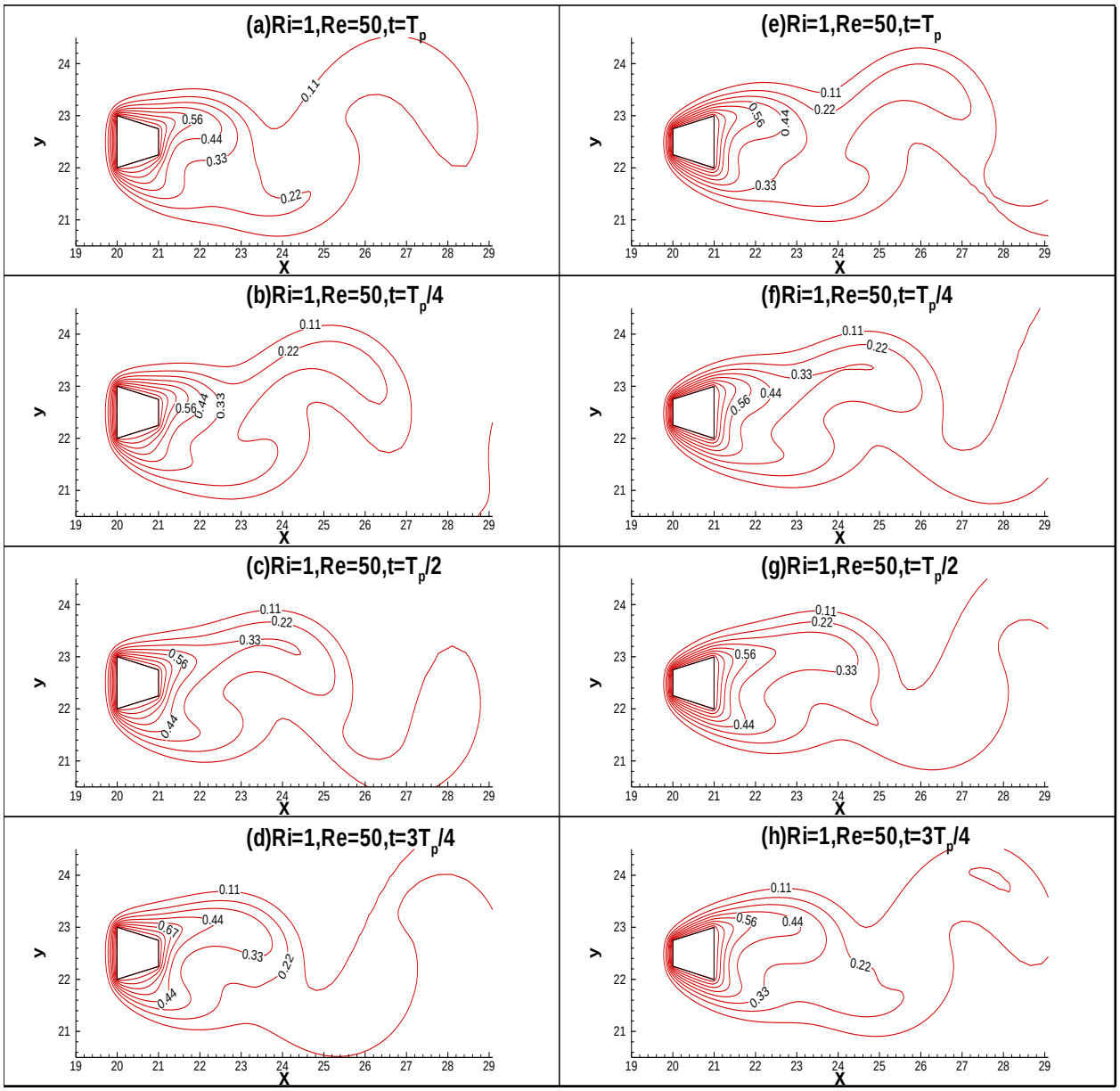

Figure 15: Isotherms for (a-d)tapered and (e-h)expanded cylinders at Ri=1 and Re=50 in periodic unsteady regime.

4.4 Instantaneous drag and lift coefficients and Nusselt number

Drag coefficient, lift coefficient and Nusselt number at Re=50 and Ri=0.5 and 1 at different time for both expanded and tapered geometries is given in Fig. 16.While for Ri=0 i.e forced convection frequency of drag force and Nusselt number is found to be identical and twice that of lift force but in mixed convection the frequency of all these parameters are found to be identical.

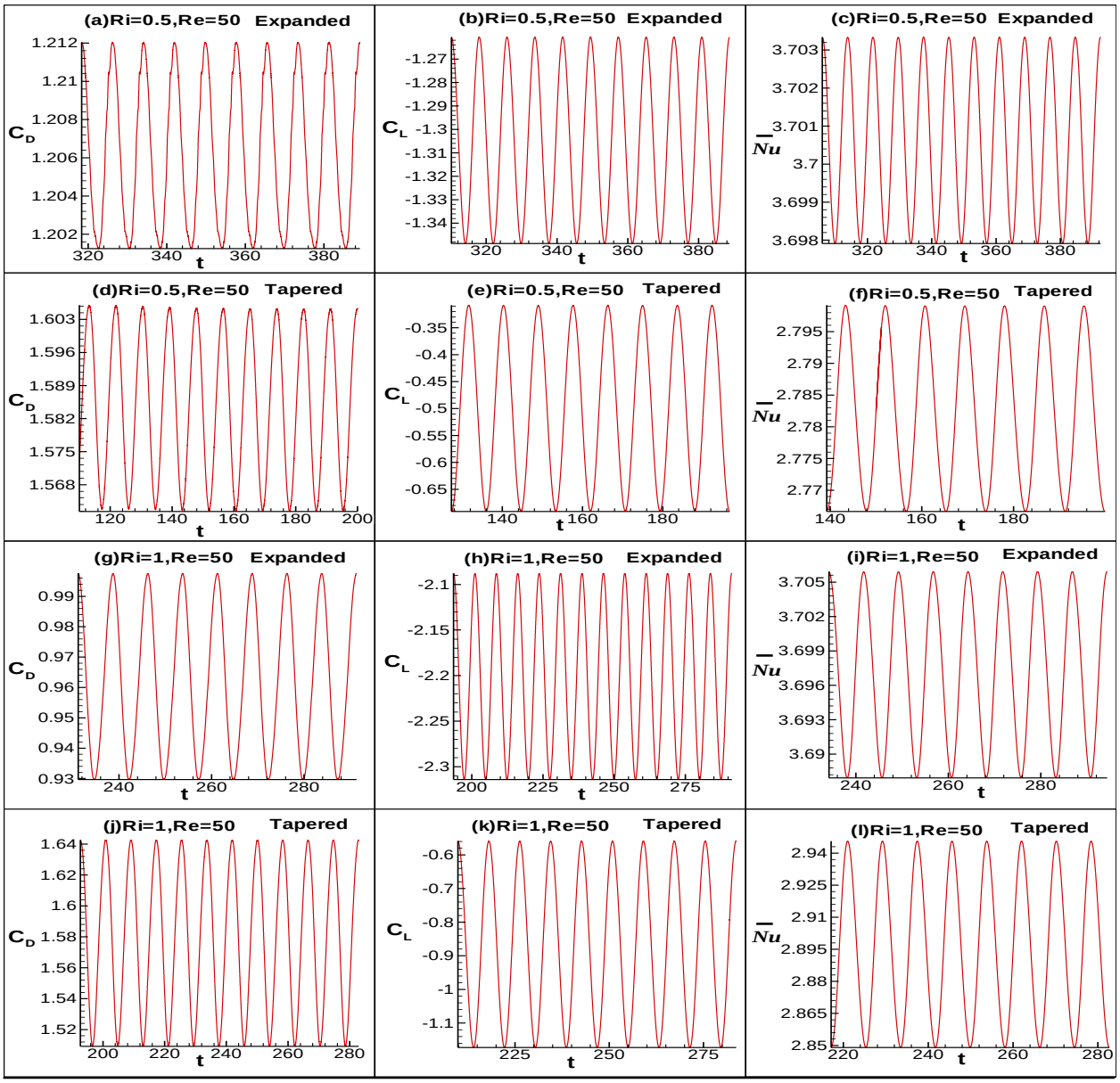

Figure 16: Time history of C_D, C_L and $\bar{Nu}$ for expanded and tapered bodies at Re=50 at different Ri.

This phenomena is due to the fact that lift force is more sensitive to change to buoyancy effects and hence frequency of lift force appreciates significantly as compared to drag and Nusselt number making all the frequency of all these parameters same. Also, on comparing tapered and expanded bodies at same operating conditions, it is found that instantaneous values of Nusselt number, drag and lift coefficients are higher for tapered body than expanded one. For the calculation of time-averaged values, instantaneous values of these output parameters for about 10 constant amplitude cycles were taken.

4.5 Time-average lift and drag coefficients

Lift arises when asymmetric flow occurs and hence for Ri=0, time-averaged lift coefficient is zero. But when cross-buoyancy effect is induced then lift forces increase and hence as we increase Ri, lift coefficient increases. Variation of lift coefficient with Reynolds number and Richardson number is given in Fig. 17. The lift coefficient is found higher for the tapered body as compared to the expanded body for same operating condition which is expected due to formation of vortices at the bottom of the tapered body as evident from streamlines given in Figs. 8-11.

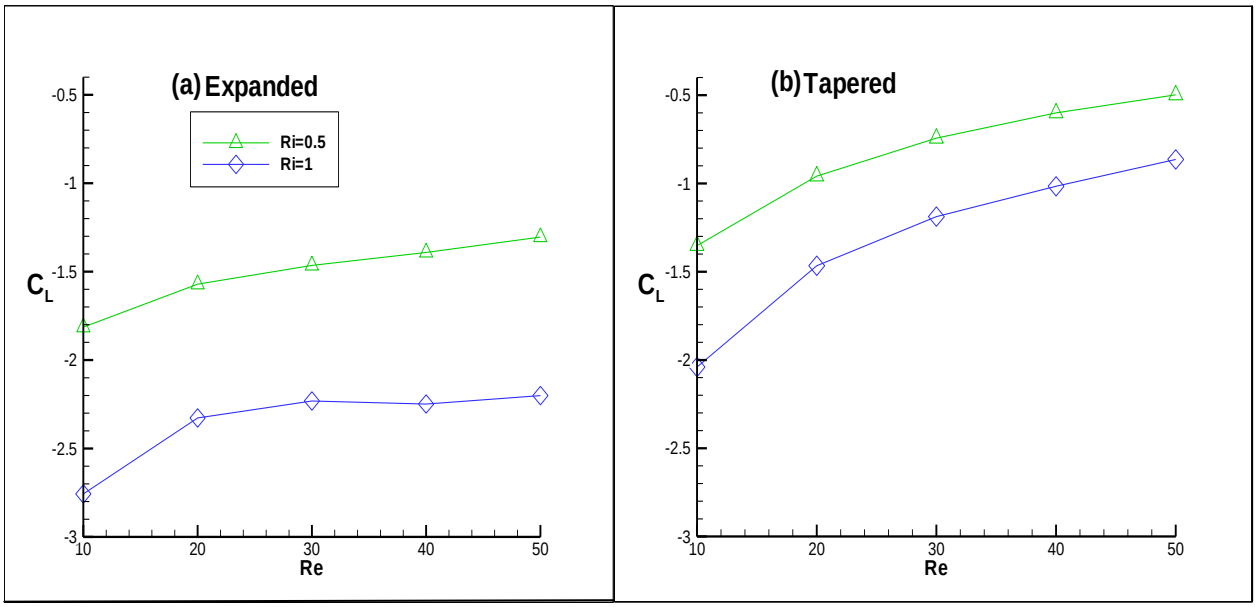

Figure 17: Variation of lift coefficients with Re and Ri for (a)expanded and (b)tapered trapezoidal bluff bodies.

Drag coefficient consists of two components- drag coefficient due to viscous force (C_{DF}) and drag due to pressure difference (C_{DP}). C_{DF} is the component of drag parallel to the flow while C_{DP} is the component of drag acting perpendicular to the flow. Summation of both of these forces gives total drag on an object due to moving fluid. Main component of overall drag force is drag due to viscous in a streamline body because of attachment of fluid particles to the surface of cylinder for larger time due to delay in flow separation. While for a bluff body drag due to pressure dominates as in bluff body drag mainly occurs due to pressure differences occurring due introduction of bluff body in the flow. A comparison of individual drag coefficients (drag due to viscous and drag due to pressure) and total drag coefficient between expanded and tapered geometries is provided in Fig. 18.

It is evident from Fig. 18 that drag coefficient due to friction is higher for the expanded body than the tapered body because the flow separation in expanded trapezoidal cylinder occurs from rear end in contrast to tapered trapezoidal body where flow separation happens at frontal edge. Hence, fluid particles are attached to the surface of expanded trapezoidal cylinder for a larger time as compared to tapered trapezoidal body which leads to increase in drag coefficient due to friction. On the other hand, drag coefficient due to pressure is higher for the tapered geometry as compared to the expanded geometry at same operating conditions because tapered body has larger frontal area which provides larger obstruction to flowing fluid causing an increase in pressure gradient along the obstacle. Due to this larger pressure gradient drag due to pressure increases in case of tapered geometry.

In steady regime, both C_{DF} and C_{DP} decrease with increase in Re and hence the same is the trend for overall drag coefficient. Hence the results are in congruous with the the results obtained by Dhiman and Ghosh [19] and Dhiman and Hasan [15]. But in periodic unsteady regime, drag coefficient increases and rate of increment is larger at higher Richardson number, and this explains the crossing of lines of total drag coefficient at a given Ri for the tapered body (Fig. 18f). As overall drag coefficient at Ri increases more as compared to Ri=0.5 and Ri=1 so drag coefficient curve at Ri=1 crosses the curves at other Ri. Also, for a given Reynolds number in steady regime, at the given range of Richardson number both individual and overall drag coefficients decrease for both the geometries, but in unsteady state the phenomena may reverse because rate of increase in drag coefficients in unsteady region increases with increase in Richardson number.

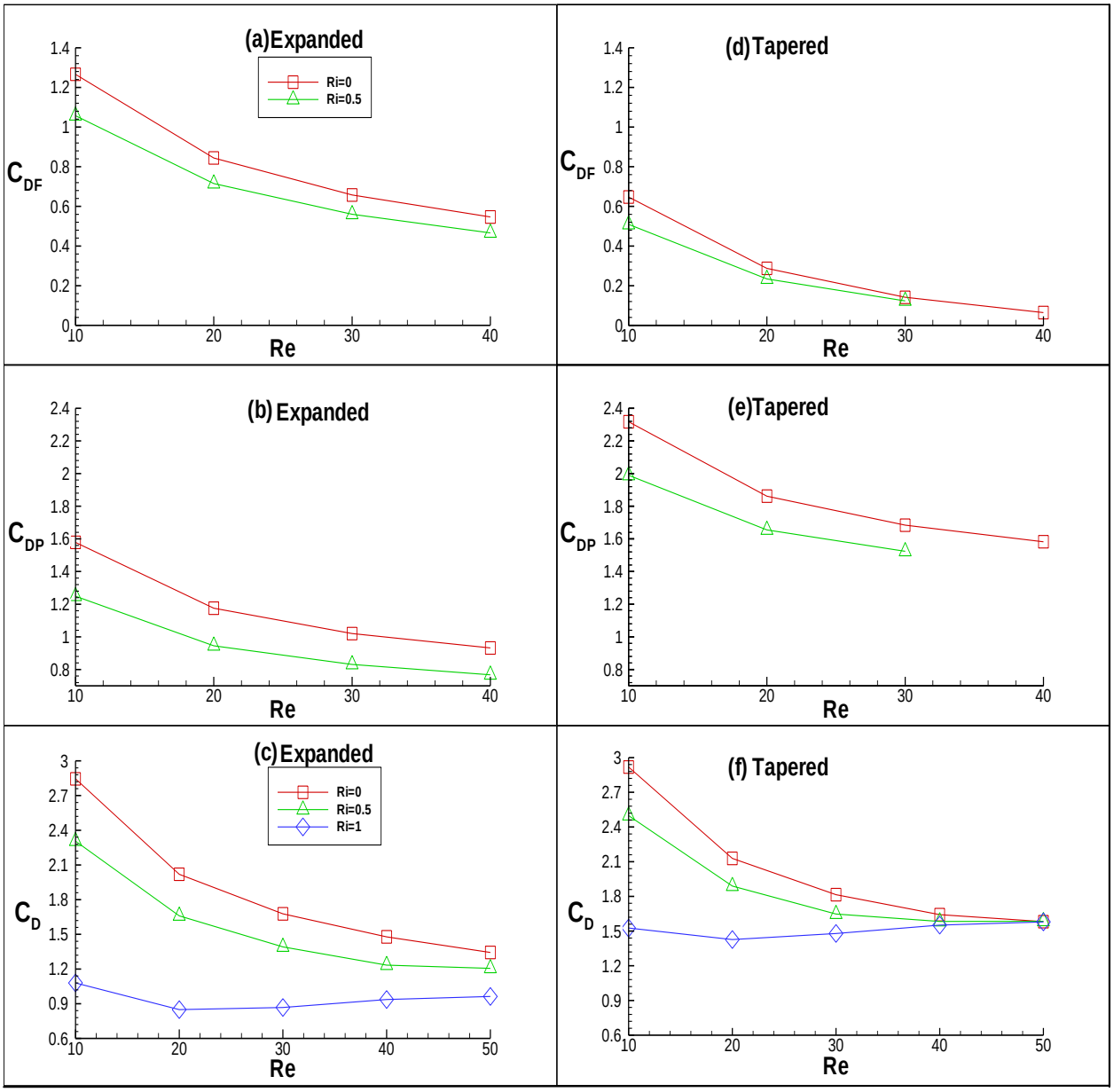

Figure 18: Comparison of drag coefficients for (a-c)expanded and (d-f)tapered trapezoidal cylinders at different Re and Ri.

4.6 Strouhal number

Strouhal number is a property that comes into play when flow is oscillatory, and indicates the amount of oscillation occurring in the system. In the current study, it is calculated from the frequency of oscillation observed in lift coefficient. A comparison of St at different values of Re for both expanded and tapered geometries is given in Fig.19. It is observed that frequency of oscillation increases with increase in Re.

For Ri=1**,** at low Re (<20) Strouhal Number is higher for tapered geometry but difference between the corresponding values of St for expanded and tapered trapezoidal cylinder at same Re decreases. For Re ≥30, Strouhal number is observed to be higher for expanded trapezoidal cylinder and difference enlarges with advancement in Reynolds number. Even for Ri=0.5, Strouhal number for expanded trapezoidal cylinder at Re=50 is observed to be higher than that of tapered geometry at same operating conditions. Hence at high Reynolds number, Strouhal number is higher for expanded geometry with respect to tapered geometry for both forced convection as well as mixed convection.

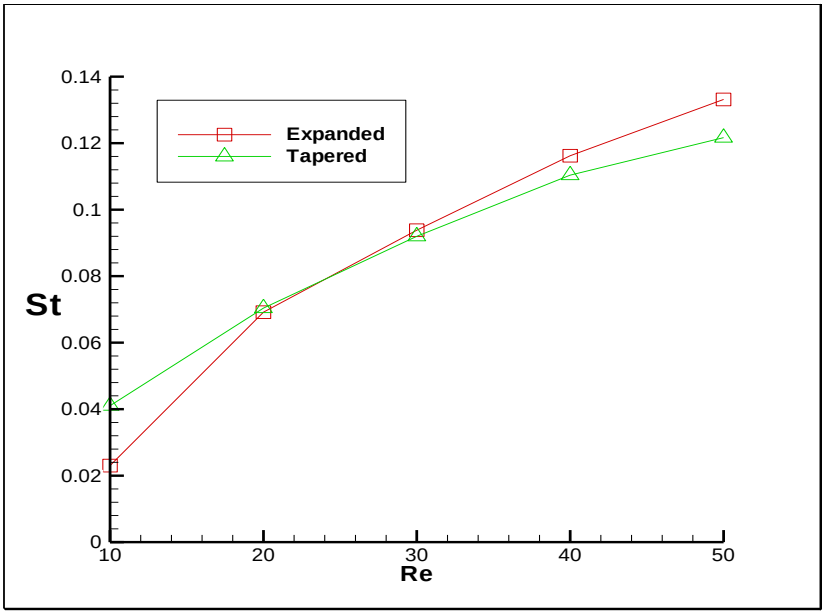

Figure 19: Variation of St with Re for expanded and tapered geometries at Ri=1.

4.7 Local and average Nusselt Numbers

Variation in local Nusselt number around the surfaces of expanded and tapered geometries for Ri=0 can be obtained from [15, 19]. For Ri=0.5 and 1 local Nusselt number has been given in Figs. 20 and 21 respectively. It is evident from the figures that maxima of local Nusselt number lies at the corners of both expanded and tapered geometries due to sharp temperature gradient at these corners. Variation of local Nusselt number in periodic unsteady

state around the obstacle at different time suggests that effect of fluctuating vortices is more prominent in rear end of cylinder while in front edge the effect is negligible for both the obstacles. The local minima of these Nusselt number lies somewhere between the edges for both expanded as well as tapered geometries.

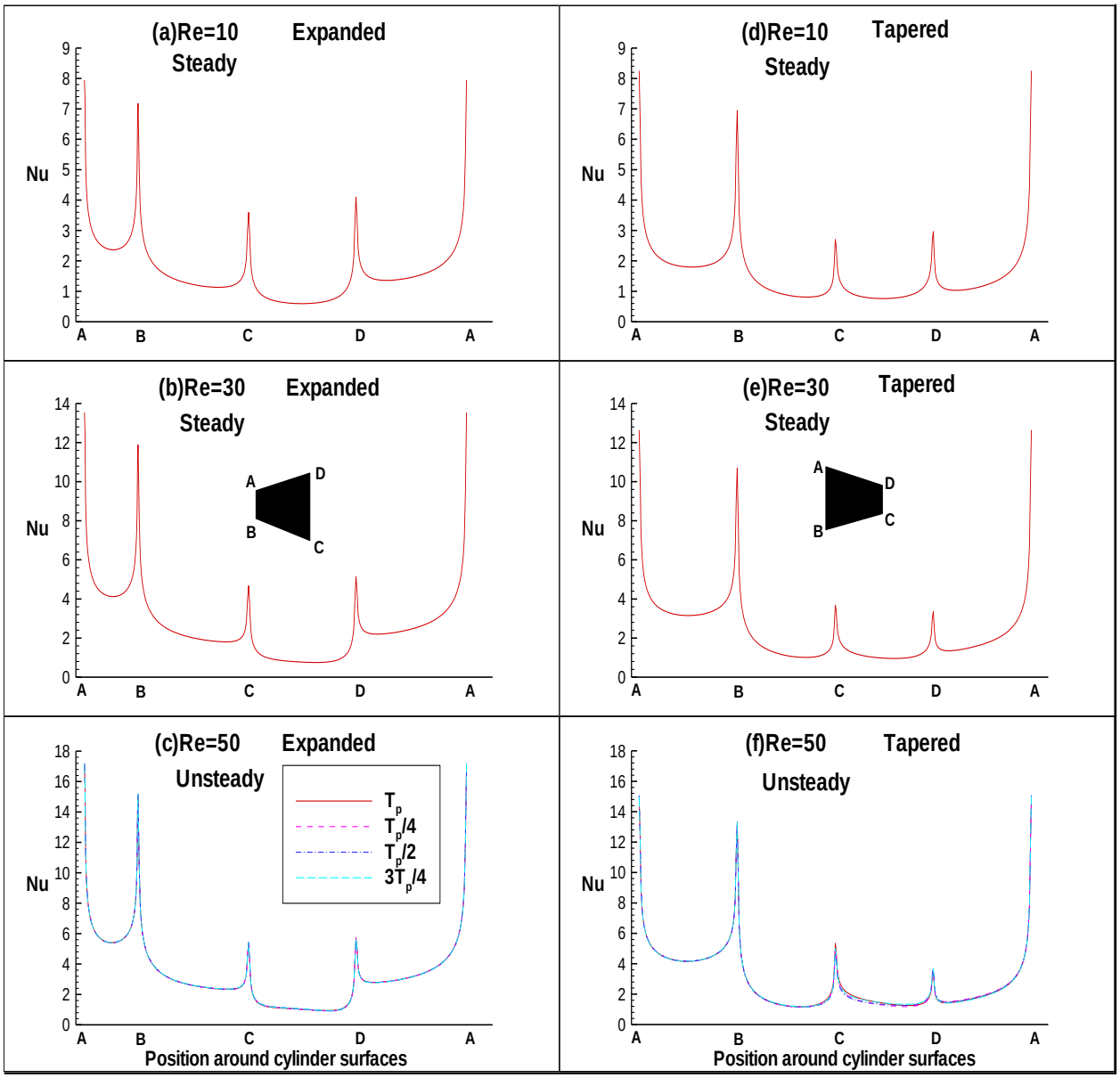

Figure 20: Local Nusselt number around (a-c)expanded and (d-f)tapered geometries at Ri=0.5.

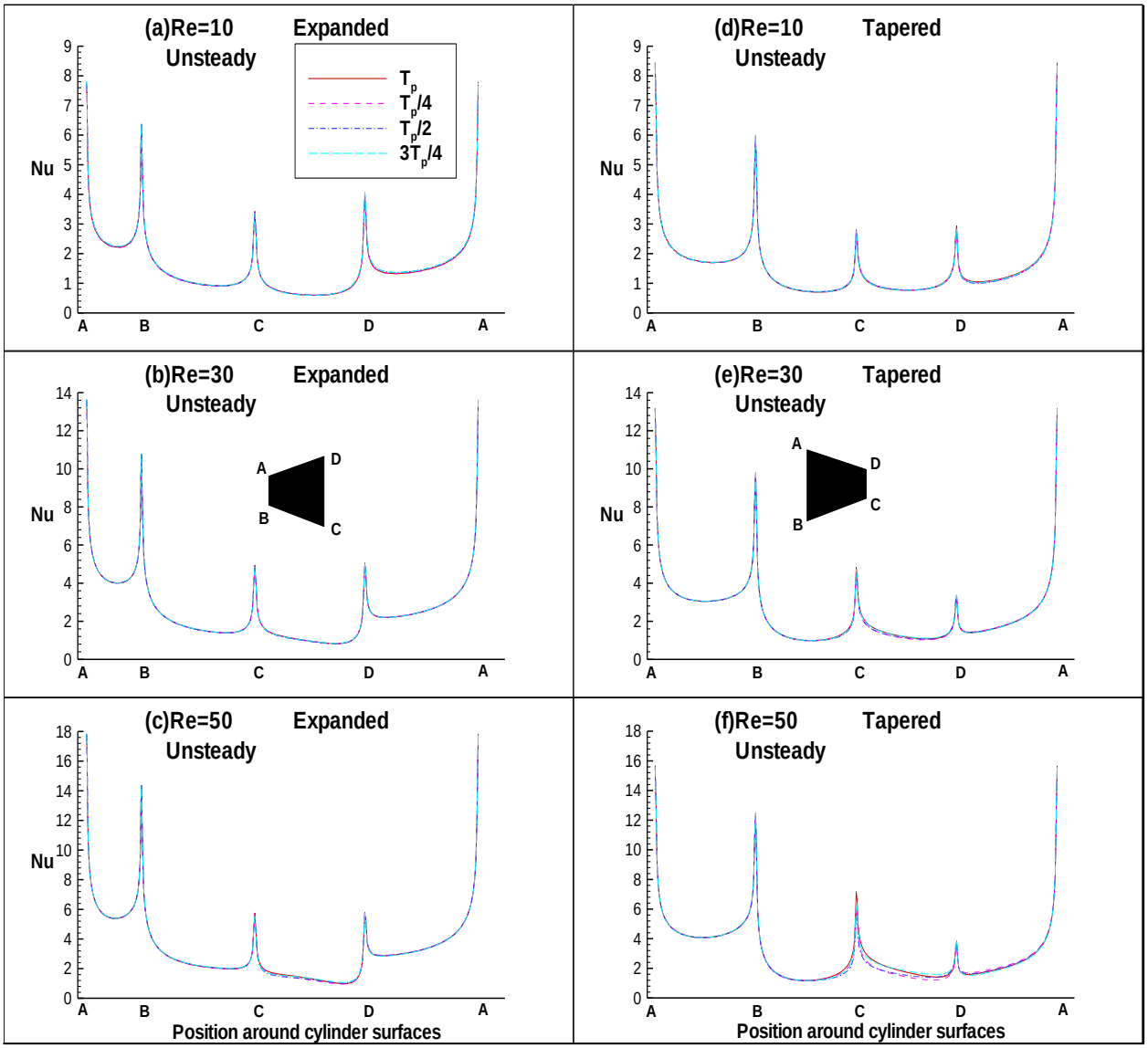

Figure 21: Local Nusselt number around (a-c)expanded and (d-f)tapered geometries at Ri=1.

Higher average Nusselt number indicates larger rate of heat transfer and with increase in periodic nature average Nusselt number is observed to increase because eddies carry heat from the body to the fluid at a faster rate. By augmenting Re, flow becomes periodic unsteady average Nusselt number also increases. A comparison of average $\bar{Nu}$ at various Re and Ri for expanded and tapered geometries has been depicted in Fig. 22. From the figure, it can be observed that although average Nusselt number increases with Re for both geometries, but average $\bar{Nu}$ is higher for the expanded body as compared to the tapered body due to delay in flow separation in

expanded body giving more time to fluid particles to exchange heat. For the expanded body Nusselt number is inversely related to Ri for all present set of conditions taken. But the difference between Nusselt number at successive Ri is decreasing with increase in Re. For tapered geometry, it is found that for low Re (<20) Nusselt number shows inverse relationship with Ri with the difference between Nusselt number at successive Ri decreasing with advancing Re. For Re>40, there is trend reversal and for constant Re, increase in Ri cause Nusselt number to increase. The reason for trend reversal can be attributed to the fact that increase in average $\bar{Nu}$ with respect to Re is higher at higher Richardson number.

It is observed that for expanded body, maximum heat transfer occurs from front surface of expanded cylinder while minimum heat transfer occurs from the rear end for all range of operating conditions in present study. In case of tapered trapezoidal body, maximum heat transfer occurs from the front surface of tapered cylinder for athwart range of operating conditions taken and minimum heat transfer occurs from rear end of tapered cylinder for all set of conditions taken except at Ri=1, Re=50 where minimum heat transfer happens from bottom surface of tapered trapezoidal cylinder.

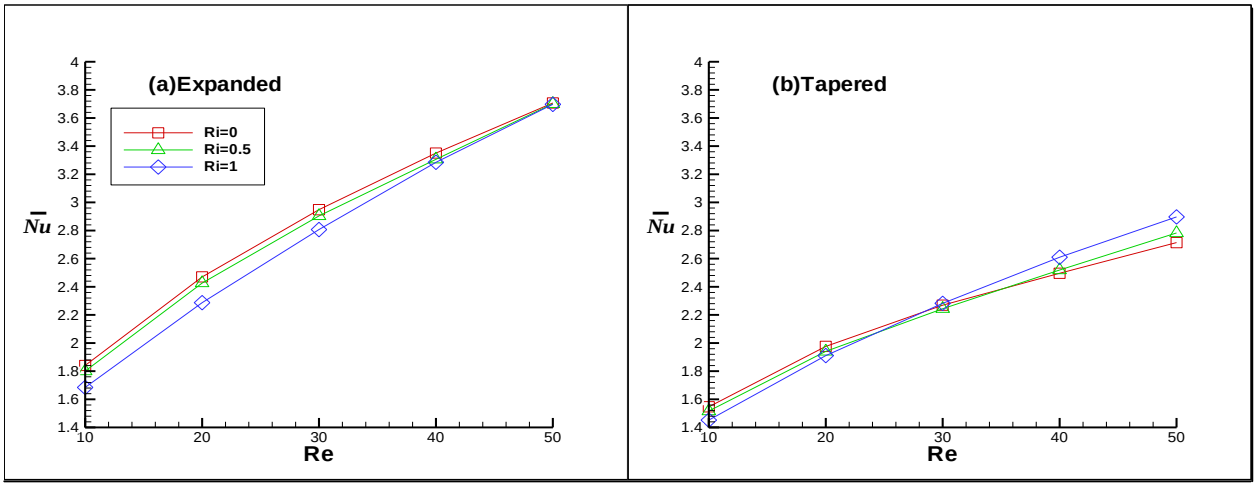

Figure 22: Variation of $\bar{Nu}$ with Re and Ri for (a)expanded and (b)tapered geometries.

The maximum percentage heat transfer enhancement for the expanded body at Ri=0.5 and Ri=1 with respect to Ri=0 is found to be approximately 8.5% and 2% respectively and this maximum value is obtained at Re=10. Similarly, for the tapered body, the maximum percentage increase in heat transfer at Ri=0.5 and Ri=1 compared to Ri=0 is found to be approximately 6%

and 2% respectively at Re=50. Table 7 provides percentage heat transfer enhancement for both the geometries at Ri=0.5 and Ri=1 compared to Ri=0 for various Re. It can be observed that percentage heat transfer enhancement decrease with increase in Re for expanded geometry but antithesis is the case for tapered body except at Re 10 and 20 where it increases. The maximum heat transfer enhancement for the tapered body compared to expanded body at Ri=0, 0.5 and 1 is found to be at Re=50 and the percentage increase in heat transfer was found to be approximately 26%, 24% and 21% respectively. Table 8 provides percentage heat transfer enhancement for tapered body as compared to expanded body for different Ri and Re. As we move from expanded to tapered geometry percentage heat transfer increase with increase in Re for all Ri. While percentage enhancement factor is high at lower Ri for same Re, hence increasing Ri keeping Re constant decrease percentage enhancement factor.

Table 7: Percentage heat transfer enhancement (E.F) for expanded and tapered cylinder at various Re.

Re	E.F at Ri=0.5 w.r.to Ri=0		E.F at Ri=1 w.r.to Ri=0	
	Expanded	Tapered	Expanded	Tapered
10	2.2	1.9	8.4	6.1
20	1.7	1.7	7.4	3.3
30	1.5	1.1	4.7	0.5
40	1.3	0.9	1.9	4.5
50	0.1	2.5	0.2	6.7

Table 8: Percentage heat transfer enhancement for expanded body with respect to tapered at various Ri.

Re	Ri=0	Ri=0.5	Ri=1
10	15.9	15.7	13.8
20	20.1	20.0	16.4
30	23.0	22.7	18.6
40	25.4	23.8	20.5
50	26.7	24.8	21.6

Finally, an empirical correlation to obtain the $\bar{Nu}$ for the range of operating conditions chosen in this study is established as follows-

$\bar{Nu}$ =(0.6149-0.01993*Ri)*$Re^{0.4616}$ (R^2=0.9961) (for expanded trapezoidal cylinder) (5)

$\bar{Nu}$ =(0.6033+0.01339*Ri)*$Re^{0.3878}$ (R^2=0.9909) (for tapered trapezoidal cylinder) (6)

Maximum error obtained from Eqs. (5) and (6) in case of the expanded geometry is about 3.7% at Ri=1, Re=20 and similarly for the tapered geometry maximum deviation is observed to be about 4.7% at Ri=0, Re=10.

CHAPTER 5

CONCLUSIONS

A two-dimensional numerical simulation of flow across trapezoidal bluff body (expanded and tapered) is performed for the following range of control parameters: Re=10-50, Ri=0-1 and Pr=0.7. It was found that for a given Richardson number, an increase in Reynolds number increases the drag coefficient in periodic unsteady regime, but in steady regime these coefficients decrease with increase in Re. Drag coefficient and average Nusselt number is higher for the expanded trapezoidal cylinder as compared to the tapered trapezoidal cylinder due to streamline nature of expanded geometry. At low Re, on increasing Richardson number, the values of drag coefficient decreases, but antithesis is the case at high Re. Although at low Re, $\bar{Nu}$ varies inversely with Ri but as Re increases there is trend reversal. Critical Re is found to decrease with increase in Ri, because of higher periodic nature caused by cross-buoyancy. Strouhal number increases with increase in Reynolds number thus making the system more oscillatory in nature. St is found higher for the expanded geometry at high Re and the difference increases with increase in Re. Lift force comes into act in cross-buoyancy case where the flow is asymmetric and at higher value of Ri, C_L is found to decrease for same Re. Lift coefficient is found higher for the tapered body as compared to the expanded body for the same operating condition; this behavior is because of vortex formation beneath the tapered body. Maximum heat transfer enhancement for the expanded body at Ri=0.5 and Ri=1 compared to Ri=0 is found to be approximately 8.5% and 2% respectively. Similarly, for the tapered body, maximum augmentation in heat transfer for the above mentioned conditions is found to be approximately 6% and 2%. Maximum heat transfer enhancement for the tapered body compared to the expanded body at Ri=0, 0.5 and 1 is found to be approximately 26%, 24% and 21% respectively.

References

[1] G. L. Pankanin, The vortex flowmeter: various methods of investigating phenomena, Meas. Sci. Technol., 16 (2005) R1 – R16.

[2] N. Steggel, N. Rockliff, Simulations on the effects of body shape on lock in characteristics in pulsating flow by the discrete vortex method, J. Wind Eng. Ind. Aerodyn., 69–71 (1997) 317–321.

[3] J. J. Miau, J. T. Wang, J. H. Chou, C.Y. Wei, Low frequency fluctuation in the near wake region of a trapezoidal cylinder with low aspect ratio, J. Fluids Structures, 17 (2003) 701-715.

[4] J. Xing, T. Zhang, Y. Hu, Optimisation of the bluff body in vortex flow meter, Proc. 7th World Congress on Intelligent Control and Automation, Chongqing, China (2008).

[5] A. K. El-Wahed, M. W. Johnson, J. L. Sproston, Numerical study of vortex shedding from different shaped bluff bodies, Flow. Meas. Instrum., 4 (1993) 233-240.

[6] A. Venugopal, A. Agarwal, S. V. Prabhu, Influence of blockage and upstream disturbances on the performance of vortex flow meter with trapezoidal bluff, Measurement, 43 (2010) 954 - 964.

[7] D. Wang, H. Pham, C. Chao, J. M. Chen, A piezoelectric energy harvester based on pressure fluctuations in Karman vortex street, World Renewable Energy Congress, Linkoping, Sweden (2011).

[8] A. H. Gee, N. E. Houghton, G. M. Treece, R. W. Prager, A mechanical instrument for 3d ultrasound probe calibration, Ultrasound Med. Biol., 31 (2005) 505–581.

[9] S. Goujon-Durand, K. Renffer, J. E. Wesfreid, Downstream evolution of the Bernard von Karman instability, Phy. Rev. E, 50 (1994) 308 – 313.

[10] J. P. Hulin, C. Fierfort, R. Coudol, Experimental study of vortex emission behind bluff obstacles in a gas liquid vertical two-phase flow, Int. J. Multiphase Flow, 8 (1982) 475-490.

[11] T. S. Lee, Early stages of an impulsively started unsteady laminar flow past tapered trapezoidal cylinders, Int. J. Numer. Methods Fluids, 26 (1998) 1181-1203.

[12] Y. J. Chung, S. -H. Kang, Laminar vortex shedding from a trapezoidal cylinder with different height ratios, Phy. Fluids, 12 (2000) 1251 -1254.

[13] R. Kahawita, P. Wang, Numerical simulation of the wake flow behind trapezoidal bluff bodies, Comp. Fluids, 31 (2002) 99-112.

[14] A. Venugopal, A. Agarwal, S. V. Prabhu, Influence of blockage and shape of a bluff body on the performance of vortex flow meter with wall pressure measurement, Measurement, 44 (2010) 954 – 964.

[15] A. Dhiman, M. Hasan, Flow and heat transfer over a trapezoidal cylinder: steady and unsteady regimes, Asia-Pacific J. Chem. Eng., 8 (2013) 433-446.

[16] A. Dhiman, S. Verma, R. Ghosh, Laminar momentum and heat transfer in a channel with a built-in tapered trapezoidal bluff body, Heat Transfer-Asian Research, (2014), in press.

[17] T. S. Lee, Numerical study of early stages of an impulsively started unsteady laminar flow past expanded trapezoidal cylinders, Int. J. Numer. Methods Heat Fluid Flow, 8 (1998) 934-955.

[18] X. B. Chen, P. Yu, S. H. Winoto, H. T. Low, Numerical analysis for the flow past a porous trapezoidal cylinder based on the stress-jump interfacial conditions, Int. J. Numer. Methods Heat Fluid Flow, 19 (2009) 223-241.

[19] A. Dhiman, R. Ghosh, Computer simulation of momentum and heat transfer across an expanded trapezoidal bluff body, Int. J. Heat Mass Transfer, 59 (2013) 338 – 352.

[20] N. Sharma, A. K. Dhiman, S. Kumar, Mixed convection flow and heat transfer across a square cylinder under the influence of aiding buoyancy at low Reynolds numbers, Int. J. Heat Mass Transfer, 55 (2012) 2601-2614.

[21] N. Sharma, A. Dhiman, S. Kumar, Power-law shear-thinning flow around a heated square bluff body under aiding buoyancy at low Reynolds numbers, Korean J. Chem. Eng., 31 (2014) 754-771.

[22] D. Chatterjee, S. Amiroudine, Two-dimensional mixed convection heat transfer from confined tandem square cylinders in cross-flow at low Reynolds numbers, Int. Comm. Heat Mass Transfer 37 (2010) 7–16.

[23] D. Chatterjee, B. Mondal, Mixed convection heat transfer from tandem square cylinders for various gap to size ratios, 63 (2013) 101-119.

[24] R. B. Bird, W. E. Stewart, E. N. Lightfoot, Transport Phenomena, 2nd edition, Wiley, New York, 2001.

[25] ANSYS, Inc., 2009, ANSYS FLUENT 12.0 User's Guide, U.S.A.